ION CYCLOTRON WHISTLERS*

by

D. A. Gurnett**

A dissertation submitted in partial fulfillment of the requirements for the degree of Doctor of Philosophy in the Department of Physics and Astronomy in the Graduate College of the University of Iowa

June 1965

Chairman: Professor J. A. Van Allen

*Research supported in part by the U. S. Office of Naval Research under Contracts N9onr 93803 and Nonr 1509(06).

**NASA Graduate Research Fellow.

ACKNOWLEDGEMENTS

The author would like to express his sincere appreciation to Professor J. A. Van Allen for his interest in this study, to Professor N. M. Brice and Dr. R. L. Smith for their critical comments, and to Professor R. A. Helliwell for his helpful discussions. The author also wishes to express his indebtedness to Mr. Stan Shawhan for his contribution to the experimental aspects of this study, to Mr. George Frohwein and Mr. A. D. Maroff for their assistance in technical matters, to Professor J. F. Curtis for the use of the Speech Pathology and Audiology Department's Sonograph, and to Mrs. Evelyn Robison for typing this manuscript.

The research at the University of Iowa was supported by the Office of Naval Research under contracts N9onr-93803 and Nonr 1509(06).

FORWARD

In this paper I present an explanation of a new VLF phenomenon based on the effects of ions on the propagation of an electromagnetic wave in the ionosphere. This explanation is the result of an independent study of propagation in multicomponent plasmas and its application to the new phenomenon.

This investigation was stimulated by the discovery of an ion gyrofrequency phenomenon in the Alouette I and Injun III data (June, 1963). This discovery was announced in Nature: "An Ion Gyrofrequency Phenomenon Observed in Satellites" by R. L. Smith, N. M. Brice, and J. Katsufrakis of Stanford University; D. A. Gurnett and S. D. Shawhan of the University of Iowa; and J. S. Belrose and R. E. Barrington of the Defence Research Telecommunications Establishment, Ottawa, Ontario, Canada. Since the discovery of this new phenomenon I have worked out the propagation equations for a multicomponent plasma in the form presented in this dissertation and applied these equations to propagation in the ionosphere in order to explain this new phenomenon, herein called a proton-whistler. This theory of the proton-whistler and data supporting the theory were presented

at my Ph.D. oral examination September 30, 1964. In a recent paper by Smith and Brice (fall URSI meeting October 12-17, 1964; and published in J. Geophys. Res., 69, 5029-5040, 1964) an important feature of the explanation of the proton-whistler (the polarization reversal condition) was presented. In this thesis I discuss the polarization reversal condition because I derived it independently of Brice and Smith and because it is an important aspect of the explanation of the proton-whistler phenomenon. This theory of the proton-whistler has been submitted for publication to the J. Geophys. Res. as a joint paper "Ion Cyclotron Whistlers" by D. A. Gurnett, S. D. Shawhan, N. M. Brice, and R. L. Smith.

TABLE OF CONTENTS

TABLE OF CONTENTS
(continued)

ABSTRACT

An experimental study of the proton-whistler, a new VLF phenomenon observed in satellite data, is presented and an explanation of this new effect is given.

The proton-whistler appears on a frequency-time spectrogram as a tone which starts immediately following the reception of a short fractional-hop whistler at the satellite and initially shows a rapid rise in frequency, asymptotically approaching the gyrofrequency for protons in the plasma surrounding the satellite.

It is proposed that the proton-whistler is simply a dispersed form of the original lightning impulse and that the dispersion can be explained by considering the effect of ions on the propagation of an electromagnetic wave in the ionosphere. The propagation of a wave in a multicomponent plasma for frequencies on the order of the ion gyrofrequencies is discussed using the notation used by Stix [1962]. In the ionosphere it is found that in addition to the right-hand polarized whistler mode the left-hand polarized mode (ion cyclotron wave) is also a possible mode of propagation for certain ranges of frequencies and altitudes. Between each adjacent ion gyrofrequency there is a frequency for which both modes of propagation are linearly polarized. These frequencies are called the crossover frequencies.

A wave propagating in the ionosphere changes polarization at the altitude for which the wave frequency is equal to a crossover frequency. This polarization reversal provides the mechanism by which an upgoing whistler can become an ion cyclotron wave. We show that the proton-whistler is an ion cyclotron wave which occurs via this polarization reversal process. The crossover frequency can be measured from spectrograms of proton-whistlers and is used to determine the fractional concentration $\alpha = n(H^+)/n_e$ in the plasma surrounding the satellite.

Near the altitude and frequencies for which polarization reversal occurs it is shown that the right-hand polarized wave and the ion cyclotron wave may be strongly coupled. For frequencies on the order of the ion gyrofrequencies this coupling process plays an important part in determining what regions of the ionosphere are accessible to waves from a given source location.

1. INTRODUCTION

A new very-low frequency (VLF) phenomenon associated with the propagation of whistlers in the ionosphere has been found in the VLF recordings from the Injun III and Alouette satellites [Smith et al., 1964] [Brice, 1964]. The new effect appears on a frequency-time spectrogram as a tone which starts immediately following the reception of a short fractional-hop whistler at the satellite and initially shows a rapid rise in frequency, asymptotically approaching the gyrofrequency for protons in the plasma surrounding the satellite. An illustration of this new phenomenon and the nomenclature that will be used in this discussion is presented in Figure 1.

It is proposed that this new phenomenon is simply a dispersed form of the original lightning impulse and that the dispersion can be explained by considering the effects of ions on the propagation of an electromagnetic wave in the ionosphere. In this paper the characteristic tone occurring immediately following the reception of a whistler is called a proton-whistler or p-whistler [see Figure 1]. The designation proton-whistler has been adopted because the phenomenon is postulated to be a whistler* and the

---

*VLF phenomena whose source of energy is a lightning impulse are classified as whistlers [Gallet, 1959].

frequency of the tone is found to asymptotically approach the gyrofrequency for protons at the point of observation. Here the short fractional-hop whistler which immediately precedes the proton-whistler is called an electron-whistler or e-whistler /see Figure 1/. The designation electron-whistler has been adopted because the electron gyrofrequency is the upper frequency limit for which the right-hand polarized whistler mode can propagate. The general consistency of this terminology will become evident.

The explanation of the p-whistler is based on calculations of the propagation of a VLF electromagnetic wave in a model ionosphere having several types of ions. Propagation in a plasma containing several ions has been considered by Hines /1957/, Buchsbaum /1960/, Stix /1962/, Yakimenko /1962/, Gintsburg /1963/, and Smith and Brice /1964/. When the effects of ions are included in the propagation equations, it is found that in addition to the right-hand polarized whistler mode the left-hand polarized mode is also a possible mode of propagation for certain ranges of frequencies and altitudes in the ionosphere. Stix /1962/ calls the left-hand polarized wave propagating at frequencies less than the maximum ion gyrofrequency an Ion Cyclotron Wave. Gintsburg /1963/ showed that the ion cyclotron mode has resonances at each ion gyrofrequency. Propagation is

possible in the ion cyclotron mode for a band of frequencies below each ion gyrofrequency and the lower cutoff frequency for each band is greater than the next lower ion gyrofrequency. The bandwidth available depends upon the relative concentrations of the various ions. We interpret the p-whistler as an ion cyclotron wave propagating in the frequency band available just below the proton gyrofrequency. Here this wave is called a Proton Cyclotron Wave.

Stix [1962] has indicated that when a plasma has positive ions having different charge to mass ratios the polarization of a wave may change sense of rotation while propagating through a slowly varying medium. Smith and Brice [1964] find that between each adjacent ion gyrofrequency there is a frequency, called the crossover frequency, for which both modes of propagation are linearly polarized. A wave propagating in a slowly varying medium changes sense of polarization when the wave frequency becomes equal to a crossover frequency. In the ionosphere this polarization reversal provides the mechanism by which an upgoing right-hand polarized e-whistler can become a left-hand polarized p-whistler. Polarization reversal is a necessary point in the explanation of the p-whistler because, as will be shown in Section 4, the predominance of O^+ and He^+ in the lower ionosphere prevents the direct propagation of a lightning impulse to the satellite entirely via the proton cyclotron mode.

In Section 4 it is shown that near the altitude and frequencies for which polarization reversal occurs the conditions may exist for strong coupling between the two modes of propagation. When strong coupling exists we can expect an upgoing e-whistler to be split into two upgoing waves. Continuing to higher altitudes these two waves propagate independently, one propagating in the right-hand polarized mode and the other in the ion cyclotron mode. This coupling process plays an important part in determining what regions of the ionosphere are accessible to waves from a given source location.

In Section 5, using a model ionosphere consisting of three ions (H^+, He^+, O^+), the evidence that proton-whistlers are ion cyclotron waves is presented. Group propagation times based on this model ionosphere show that it is consistent to interpret the p-whistler as propagating in the proton cyclotron mode and simply a dispersed form of the original lightning impulse. The dispersion of the p-whistler arises from propagation part of the distance to the satellite in the right-hand polarized mode, and part in the proton cyclotron mode. The crossover frequency can be easily determined from spectrograms of proton-whistlers and is used to make estimates of the fractional concentration of H^+ in the plasma surrounding the satellite.

In Section 6 other phenomena related to the presence of ions in the ionosphere are discussed. In the Alouette 1 satellite, using a dipole antenna, an unusual band of noise has been reported by Barrington and Belrose [1963]. This noise band has a sharp lower frequency cut-off which usually increased in frequency with decreasing latitude of the satellite. Brice and Smith [1964] have suggested that this noise band is related to the lower hybrid resonance for the ambient plasma. In the Injun III satellite, using a loop antenna, this noise band has also been observed, though much less frequently than in the Alouette data. The relatively infrequent observation of this noise band by Injun III is thought to be related to the orientation of the Injun III loop antenna relative to the geomagnetic field.

In the VLF recordings from Injun III bands of noise having frequencies as low as 180 c/s have been observed. It is thought that the banded structure of this noise is closely related to the accessibility condition imposed on waves having frequencies on the order of the ion gyrofrequencies and having sources located in the ionosphere.

2. A PRELIMINARY STUDY OF PROTON-WHISTLERS*

From the Injun III VLF experiment were obtained about 1000 hours of analog VLF data [Gurnett, 1963]. Approximately 10 percent of these data have been studied to determine the nature of the proton-whistlers observed both in the Alouette 1 and the Injun III data.

To obtain a random but reasonably sized sample of the analog VLF data all of the satellite revolutions from each ground station, recorded on the eleventh day of each of the ten months that Injun III was operable, were analyzed. Portions of sixty-seven revolutions were analyzed aurally. Twenty-three of these revolutions had proton-whistlers occurring.

The results of this preliminary study are:

(1) The proton-whistler is observed only after reception of a short fractional-hop whistler.

Figure 2 shows five spectrograms of the e-whistler trace followed by the p-whistler trace. The e-whistler is always a short fractional-hop whistler, that is, it is a whistler which has propagated only from the base of the ionosphere to the satellite. From all the spectrograms studied there has never been a case when a p-whistler was observed but an e-whistler was not. When p-whistlers are present they follow every observable short fractional-

*The experimental study presented here is a summary of a more detailed study presented in a Master's Thesis by S. D. Shawhan.

hop e-whistler. However, on only 36 percent of the revolutions for which e-whistlers were present, were p-whistlers also present.

(2) There is a frequency at which the e-whistler and the p-whistler are coincident in time.

Figure 1 shows a trace for which the e-whistler and the p-whistler are obviously coincident in time at a frequency denoted by ω_{12}. As will be shown in Section 5, this frequency corresponds to the crossover frequency between the proton gyrofrequency and the He^+ gyrofrequency. In some cases the e-whistler is cut off at a frequency Ω_c, above the starting frequency ω_{12} for the p-whistler trace (see Figure 1). In these cases it appears that the e-whistler propagation to the satellite is strongly attenuated between frequencies ω_{12} and Ω_c.

(3) The proton-whistler initially shows a rapid rise in frequency which starts at a frequency ω_{12} and asymptotically approaches the proton gyrofrequency.

To determine the value of the asymptotic frequency Ω_1 spectrograms were made on a Sonagraph (Kay Electric Co., Pine Brook, N. J.) and the frequency measured. The estimated measuring accuracy was $\pm$ 15 cps, and measurements were referenced to a standard frequency generated in the satellite. Figure 3 is a plot of the magnitude of the magnetic field B at the satellite against the asymptotic frequency. The solid curve is the calculated proton gyrofrequency. All of the experimental frequency values

lie within 3 1/2 percent of the calculated proton gyrofrequency. Most of the frequency values were lower than the proton gyrofrequency probably because the trace disappeared (~ 2 seconds after appearance) before the asymptotic value was reached. The obvious conclusion is that the asymptotic frequency is the gyrofrequency for protons in the plasma surrounding the satellite.

(4) The ratio $\omega_{12}/\Omega_1 = \Lambda_{12}$ increases with decreasing altitude approaching unity at an altitude of approximately 440 km during local midnight and at approximately 640 km during local noon.

Figure 2 (a)-(d) is a sequence of spectrograms for proton-whistlers around local midnight 20.87--24.28 L.T. With decreasing altitude the value of Λ_{12} increases from approximately 0.52 for (a) at an altitude of 874 km to approximately 0.94 for (d) (p-whistler trace marked by an arrow) at an altitude of 442 km. For altitudes below 442 km the p-whistler trace was absent. Note that the proton gyrofrequency is higher for (c) than for (d) even though (c) is higher in altitude; the value of Λ_{12} is, however, higher for (d) than for (c). This higher Ω_1 value for (c) is due to the larger value of B at the satellite; the Λ_{12} value seems to depend, therefore, on altitude and not on B.

Figure 2 (e) is a spectrogram of a local noon p-whistler. An altitude sequence of p-whistlers for local noon exhibits the

same increasing Λ_{12} with decreasing altitude found in the local midnight data. However, the Λ_{12} values are different for a given altitude with local noon values always being higher. For local midnight Λ_{12} approaches unity at approximately 440 km, whereas, for local noon, Λ_{12} approaches unity at approximately 640 km. Note that in Figure 2 (e) $\Lambda_{12} = 0.64$ which is about the same as $\Lambda_{12} = 0.69$ for (b) but (e) is at 1404 km, more than twice the altitude of (b).

(5) The proton-whistlers occur more frequently during local night than during local day and have never been observed to occur below 442 km during local night or below 640 km during local day.

In Figure 4 each open circle means that whistlers were occurring on that particular revolution within a "box" in the ionosphere 200 km by 2 hr local time. When on a particular revolution proton-whistlers were occurring, they were represented by the closed circles. The open circles, therefore, depict the whistler sample density in altitude-local time space with the occurrence of proton-whistlers superimposed as the closed circles. These data include all latitudes sampled by the satellite (see Figure 5). From Figure 4 two trends of proton-whistler occurrence can be noted. During local night, 1800-0600, there seems to be a higher frequency of occurrence of proton-whistlers than during local day, 0600-1800, while the whistler

sample density is reasonably constant for local day and night. The proton-whistlers occur at lower altitudes during the local night than they do during local day. Although the sample density of Figure 4 was about zero at altitudes below 1000 km around local noon, no proton-whistlers were found to occur below 640 km in an independent local noon (1100-1400) sample of the entire altitude range.

(6) There is an apparent Northern Hemisphere-Southern Hemisphere asymmetry in the occurrence of proton-whistlers with proton-whistlers occurring more frequently in the Northern Hemisphere than in the Southern. Also, there is an apparent high latitude cut off in the occurrence of proton-whistlers that seems to correspond to the auroral zone.

In Figure 5 the occurrence of e-whistlers (open circles) and p-whistlers (closed circles) is shown in altitude-latitude space. These data include all local times sampled by the satellite. From these data it is evident that proton-whistlers occur more frequently (relative to electron-whistlers) in the Northern Hemisphere than in the Southern Hemisphere. This asymmetry is probably due to the more frequent occurrence of lightning, the source of whistlers, in the Northern Geomagnetic Hemisphere /Handbook

of Geophysics, 1960]. In the Northern Hemisphere we would expect a greater fraction of the total number of whistlers to be short fractional-hop whistlers and consequently a greater fractional occurrence of proton-whistlers, relative to the Southern Hemisphere. Also, from Figure 5 a boundary in proton-whistler occurrence can be drawn from approximately 40° N latitude at 600 km to approximately 66° N latitude at 2700 km. This boundary is the apparent high latitude cut off in the occurrence of proton-whistlers.

3. THE PROPAGATION EQUATIONS FOR A MULTICOMPONENT PLASMA

In an effort to explain the proton-whistler phenomenon on the basis of propagation theory we now consider the effects of ions on the propagation of an electromagnetic wave in the ionosphere. As will be seen, the presence of ions having different charge to mass ratios has important effects on the propagation of an electromagnetic wave in the ionosphere for frequencies on the order of the ion gyrofrequencies.

(3.1) The Refractive Index for a Multicomponent Plasma.

The refractive index for a plasma containing several types of ions has been given by Hines [1957] and others. Here we use the symbolism introduced by Stix [1962]. Following Stix we assume a cold homogeneous plasma immersed in a uniform static magnetic field $\vec{B}_o$ and consider all first-order field quantities to vary as $\exp[i(\vec{K}\cdot\vec{r} - \omega t)]$. The refractive index is obtained from the condition for the existence of a nontrivial solution of the following set of homogeneous field equations (see Stix for the detailed derivation).

$$\begin{bmatrix} S-n^2\cos^2\theta, & -iD, & n^2\cos\theta\sin\theta \\ iD, & S-n^2, & 0 \\ n^2\cos\theta\sin\theta, & 0, & P-n^2\sin^2\theta \end{bmatrix} \begin{bmatrix} E_x \\ E_y \\ E_z \end{bmatrix} = 0 \qquad (1)$$

The magnetic field $\vec{B}_o$ is in the Z direction and $\vec{K}$ is in the X,Y plane at an angle θ with respect to $\vec{B}_o$.

The condition that Eq. (1) has a nontrivial solution is that the determinant of the matrix be zero. This condition gives the refractive index in the following form:

$$An^4 - Bn^2 + RLP = 0 \tag{2}$$

where $$A = S \sin^2 \theta + P \cos^2 \theta \tag{3}$$

$$B = RL \sin^2 \theta + PS (1 + \cos^2 \theta) \tag{4}$$

$$R = 1 - \sum_K \frac{\pi_K^2}{\omega(\omega + \epsilon_K \Omega_K)} \tag{5}$$

$$L = 1 - \sum_K \frac{\pi_K^2}{\omega(\omega - \epsilon_K \Omega_K)} \tag{6}$$

$$P = 1 - \sum_K \frac{\pi_K^2}{\omega^2} \tag{7}$$

$$S = \frac{1}{2} (R + L), \quad D = \frac{1}{2} (R - L) \tag{8}$$

$$\pi_K^2 = \frac{4\pi n_K q_K^2}{m_K} \tag{9}$$

$$\Omega_K = \left| \frac{q_K B_o}{m_K c} \right| \tag{10}$$

$$\epsilon_K = \frac{q_K}{|q_K|} \tag{11}$$

The subscripts K refer to the K-th type of particle having mass m_K, charge q_K (including sign) and number density n_K; π_K and Ω_K are the plasma frequency and gyrofrequency of the K-th constituent. The effects of collisions may be included by replacing m_K with $m_K (1 + i Z_K)$, where $Z_K = \nu_K/\omega$ and ν_K is the collision frequency for a representative particle of type K.

The solutions of Eq. (2) may be written in the following form:

$$n^2 = \frac{B \pm F}{2 A} \tag{12}$$

where $F^2 = (RL - PS)^2 \sin^4 \theta + 4P^2 D^2 \cos^2 \theta$. (13)

The waves propagating along or transverse to $\vec{B}_o$, $\theta = 0$ or $\theta = \pi/2$, are of special interest in studying general properties of Eq. (12) and are called <u>longitudinal waves</u> and <u>transverse waves</u>, respectively.

$$\text{For } \theta = 0; \quad n_R^2 = R, \qquad n_L^2 = L \tag{14}$$

$$\text{For } \theta = \pi/2; \quad n_x^2 = \frac{2RL}{R + L}, \quad n_o^2 = P \ .$$

The symbols R, L, X, and O stand for right, left, extraordinary, and ordinary.

(3.2) The Wave-Polarization.

The wave-polarization is defined in terms of the components of the electric field which lie in the wave-front. We choose the Z'-axis in the $\vec{K}$ direction, the X'-axis in the $(\vec{K}\ ,\ \vec{B}\ )$ plane, and the Y'-axis normal to the $(\vec{K}\ ,\ \vec{B}\ )$ plane. The wave-polarization is now defined:

$$\rho = \frac{E'_{Y'}}{E'_{X'}} \ . \tag{15}$$

From Eq. (1), (15), and using the appropriate coordinate transformation from unprimed to primed coordinates the wave-polarization is readily found to be:

$$\rho = \frac{i\, Dn^2 \cos\theta}{Sn^2 - RL} \ . \tag{16}$$

If ρ_o and ρ_x denote the wave-polarization for the two branches of n^2, it can be shown from Eqs. (12) and (16) that $\rho_o\rho_x = 1$.

The wave polarization gives the time dependence of the component of E perpendicular to the propagation vector. If

collisions are neglected ($Z_K = 0$) the wave-polarization is always imaginary. When $\rho = i$ the polarization is circular and field quantities varying as exp $[-i\omega t]$ rotate in the right-hand sense relative to the propagation vector. If $\rho = -i$ the polarization is circular and left-handed. For waves along B_o ($\theta = 0$) we can verify that the polarization is right circular if $n^2 = R$ and left circular if $n^2 = L$.

(3.3) Parameter Space and Wave-Normal Surfaces.

The refractive index Eq. (12) for a multicomponent plasma involves the parameters ω, B, π_1, π_2 ..., π_m and θ. The dependence of n on these parameters is conveniently studied by investigating the form of $n(\theta)$ at points in an appropriate space having scale lengths proportional to the parameters ω, B, π_1, etc. Such a plot, having an axis for each parameter being considered, is called a parameter space or C.M.A. diagram after the work of Clemmow and Mullaly [1955] and Allis [1959]. The form of $n(\theta)$ is conveniently represented by a plot of the phase velocity $u = [c/n(\theta)]$ ($\vec{K}$ /K) in spherical coordinates and is called the phase velocity surface or wave-normal surface. Wave-normal surfaces have rotational symmetry about the static magnetic field. The shape of a wave-normal surface for positive n^2 can be shown to be topologically equivalent to either a sphere,

a dumbbell lemniscoid, or a wheel lemniscoid /Stix, 1962/. The topological genera to which a given branch of n^2 belongs depends on the coordinates in parameter space.

The terms cutoff and resonance refer to the conditions for which $n^2 = 0$ and $n^2 = \infty$, respectively. The conditions for a cutoff are, from Eq. (2): $R = 0$, or $L = 0$, or $P = 0$. The resonances for the longitudinal waves are, from Eq. (14), $R = \infty$ and $L = \infty$; and for the transverse extraordinary wave, $S = 0$. The surfaces in parameter space for the cutoffs $R = 0$, $L = 0$, $P = 0$ and the surfaces for the resonances $R = \infty$, $L = \infty$, $S = 0$ have a special significance in determining the topological genera of the wave-normal surfaces. These surfaces are called bounding surfaces and they divide parameter space into a number of volumes called bounded volumes. Stix /1962/ shows the important result that for a given branch of n^2 the topological genera of the wave-normal surface is the same throughout a bounded volume. Thus if the wave-normal surfaces are determined at one point in a bounded volume they are topologically correct throughout that volume.

The wave-normal surfaces for the two branches of n^2 are conveniently labeled right (R) and left (L) according to the sense of polarization at $\theta = 0$, or ordinary (O) and extraordinary (X) according to the refractive index at $\theta = \pi/2$.

The R, L labeling scheme remains consistent throughout a bounded volume only if the surface $D = 0$ is included as a bounding surface in parameter space. The surface $D = 0$ must be included because the polarization ρ changes sign at $D = 0$ (see Eq. 16). Wave-normal surfaces can also be consistently labeled fast (f) or slow (s) according to the phase velocities at angles between 0 and $\pi/2$.

4. THE PROPAGATION OF ION CYCLOTRON WAVES IN A MODEL IONOSPHERE HAVING THREE IONS

(4.1) The Parameter Space for a Plasma Having Three Ions.

We now specialize this investigation to a plasma consisting of a neutral mixture of three types of singly charged positive ions (H^+, He^+, O^+) and electrons. These four constituents are the predominant charged particles found in the ionosphere above 200 km /Bourdeau, 1963/. Since we are interested in effects at frequencies on the order of the proton gyrofrequency we assume that the wave frequency is less than the geometric mean of the electron gyrofrequency Ω_e, and the proton gyrofrequency Ω_1, i.e., $\omega^2 < \Omega_e \Omega_1$. We also make the useful observation that in the ionosphere, above approximately 200 km, we can assume $\Omega_e \Omega_1 << \pi_e^2$. For the preliminary analysis the plasma is assumed to be collisionless ($Z_K = 0$).

Before discussing the wave-normal surfaces in parameter space, it is illuminating to consider the refractive index squared for the waves at $\theta = 0$ and $\theta = \pi/2$. Introducing the normalized frequency parameter $\Lambda = \omega/\Omega_1$, Ω_1 = proton gyrofrequency, and the concentration parameters $\alpha = n(H^+)/n_e$, $\beta = n(He^+)/n_e$, and $\gamma = n(O^+)/n_e$ we can write R, L, S, D, and P as follows ($\omega << \omega_e$):

$$R = 1 + \left(\frac{\pi_e}{\Omega_e}\right)^2 + \frac{\pi_e^2}{\Omega_1\Omega_e}\left[\frac{1}{\Lambda} - \frac{\alpha}{\Lambda(1+\Lambda)} - \frac{\beta}{\Lambda(1+4\Lambda)} - \frac{\gamma}{\Lambda(1+16\Lambda)}\right] \tag{17}$$

$$L = 1 + \left(\frac{\pi_e}{\Omega_e}\right)^2 - \frac{\pi_e^2}{\Omega_1\Omega_e}\left[\frac{1}{\Lambda} - \frac{\alpha}{\Lambda(1-\Lambda)} - \frac{\beta}{\Lambda(1-4\Lambda)} - \frac{\gamma}{\Lambda(1-16\Lambda)}\right] \tag{18}$$

$$S = 1 + \left(\frac{\pi_e}{\Omega_e}\right)^2 + \frac{\pi_e^2}{\Omega_1\Omega_e}\left[\frac{\alpha}{1-\Lambda^2} + \frac{4\beta}{1-16\Lambda^2} + \frac{16\gamma}{1-256\Lambda^2}\right] \tag{19}$$

$$D = \frac{1}{\Lambda}\frac{\pi_e^2}{\Omega_1\Omega_e}\left[1 - \frac{\alpha}{1-\Lambda^2} - \frac{\beta}{1-16\Lambda^2} - \frac{\gamma}{1-256\Lambda^2}\right] \tag{20}$$

$$P = 1 - \frac{1}{\Lambda^2}\left(\frac{\pi_e}{\Omega_1}\right)^2 \tag{21}$$

$$\alpha + \beta + \gamma = 1 \tag{22}$$

Using these equations and the refractive index squared for the longitudinal R and L-waves, and the transverse X-wave has been calculated as a function of the frequency parameter Λ and is shown in Figure 6. The concentration parameters have been fixed for this illustrative case, with $\alpha = 0.8$, $\beta = 0.15$, $\gamma = 0.05$,

and $\pi_e/\Omega_e = 1$. The refractive index squared for the transverse O-wave ($n_o^2 = P$) is a large negative quantity for the conditions being considered ($\omega^2 < \Omega_1\Omega_e$, $\pi_e^2 >> \Omega_1\Omega_e$) and is not shown in Figure 6.

The bounding surfaces shown in Figure 6 are Λ values (frequencies) corresponding to the cutoff $L = 0$, the resonances $L = \infty$ and $S = 0$, and the condition $D = 0$. Since only the parameter Λ is being considered, the bounding surfaces in parameter space reduce to points on the Λ axis and bounded volumes become intervals on the Λ axis. The resonances for the longitudinal L-wave are at the gyrofrequencies for H^+, He^+, and O^+, corresponding to $\Lambda = 1$, $\Lambda = 1/4$, and $\Lambda = 1/16$. These resonances are called the ion cyclotron resonances. The resonances for the transverse X-wave are at Λ values which are roots of $S = 0$. These transverse X-wave resonances are called hybrid resonances and have been discussed by Auer [1958], Buchsbaum [1960], Allis [1963], and Smith and Brice [1964]. The hybrid resonances occurring between the ion gyrofrequencies are called ion-ion hybrid resonances, and the hybrid resonance between the electron gyrofrequency and the highest ion gyrofrequency ($\Lambda = 27.8$ in Figure 6) is called the lower hybrid resonance. VLF noise emissions closely associated with the lower

hybrid resonance frequency have been found in the Alouette I VLF data [Brice and Smith, 1964]. Cutoffs for the longitudinal L-wave and transverse X-wave are at Λ values which are roots of $L = 0$. The refractive index squared for the longitudinal R-wave is positive for $\omega < \Omega_e$. From Figure 6 of Eq. (12) it is seen that the refractive indices of the L, R, and X-waves are equal at the bounding surface $D = 0$.

The frequencies corresponding to the roots of $D = 0$ have been discussed by Smith and Brice [1964] and are called the crossover frequencies. Stix [1962] finds that the condition $D = 0$ has a solution only when the plasma has positive ions having different charge to mass ratios, and only for frequencies greater than the minimum ion gyrofrequency and less than the maximum ion gyrofrequency. The crossover frequency between the H^+ and He^+ ion cyclotron resonances is denoted ω_{12}, and between He^+ and O^+ is denoted ω_{23} etc.

Having illustrated the cutoff and resonance frequencies for a particular set of parameters we now determine how these frequencies depend upon the parameters α, β, and π_e/Ω_e. The parameter γ is not an independent parameter since it is determined by the condition that the plasma be electrically neutral (Eq. 22). The bounding surfaces $L = 0$, $S = 0$, and

$D = 0$ have solutions for Λ which depend upon α, β, and π_e/Ω_e. First, we consider the bounding surface $D(\Lambda, \alpha, \beta) = 0$. We note that π_e/Ω_e is not a parameter for this bounding surface since it is a multiplicative factor in Eq. (20). If we consider Λ a constant, Eq. (20) becomes a linear equation in α and β. The linear relation in α and β, defined by $D(\Lambda, \alpha, \beta) = 0$, has been plotted for various Λ values and is shown in Figure 7. If values for α and β are given, the Λ values satisfying $D(\Lambda, \alpha, \beta) = 0$ can be determined by interpolating between the Λ contours.

It would be convenient if the technique used to obtain a contour plot of $D = 0$ could be applied to the equations $L(\Lambda, \alpha, \beta, \pi_e/\Omega_e) = 0$ and $S(\Lambda, \alpha, \beta, \pi_e/\Omega_e) = 0$. We note that between the ion gyrofrequencies the functions $L(\Lambda)$ and $S(\Lambda)$ cross the zero axis with a steep slope and the small term $1 + (\pi_e/\Omega_e)^2$, in Eqs. (18) and (19), can be omitted when solving for the roots of $L(\Lambda) = 0$ and $S(\Lambda) = 0$, provided that the roots are between the ion gyrofrequencies and that $\pi_e^2 >> \Omega_e\Omega_1$. With this simplification the surfaces $L = 0$ and $S = 0$ are independent of the parameter π_e/Ω_e and can be plotted as contours in the α, β plane, as shown in Figures 7 and 8. This procedure fails for the lower hybrid resonance since $S(\Lambda)$

crosses the zero axis with a small slope for Λ values greater than one. The lower hybrid resonance frequency has been given by Smith and Brice [1964] and can be derived from Eq. (19) by assuming $\Lambda >> 1$:

$$\Omega_{LH}^2 = \Omega_1 \Omega_e \frac{(\alpha + \beta/4 + \gamma/16)}{[1 + (\Omega_e/\pi_e)^2]} . \qquad (23)$$

The bounding surfaces $L(\Lambda, \alpha, \beta) = 0$, $S(\Lambda, \alpha, \beta) = 0$, and $D(\Lambda, \alpha, \beta) = 0$ intersect the $\gamma = 0$ plane in parameter space as shown in Figure 9. The $\gamma = 0$ plane gives the parameter space for a two component plasma having a fractional concentration α of H^+ ions and a fractional concentration $1-\alpha$ of He^+ ions. Using the contour plots for $L = 0$, $S = 0$, and $D = 0$ the dependence of the critical frequencies (cutoff, resonance, etc.) on the concentrations can be visualized. In Section 4.3, when a model ionosphere is considered, the bounding surface contours in Figures 7 and 8 are especially useful for determining the cutoff, hybrid resonance, and crossover frequencies as a function of altitude.

Smith and Brice [1964] have shown that the relative concentration of each of the ionic constituents of a multiple-ion plasma may be determined from a knowledge of either all the ion-ion hybrid resonances, or all the multiple-ion cutoff frequencies, or all the crossover frequencies. From the contour

plots of L = 0, D = 0, and S = 0 it would appear that, for a plasma having three types of ions, a measurement of any two of the critical frequencies (cutoffs, crossovers, and hybrid resonances) would determine the relative concentrations α, β, and γ. That this is in fact the case can be seen from the equations $D(\Lambda, \alpha, \beta) = 0$, $L(\Lambda, \alpha, \beta) = 0$, and $S(\Lambda, \alpha, \beta) = 0$.

$$\frac{255}{1-\Lambda^2}\,\alpha + \frac{240}{1-16\Lambda^2}\,\beta = 256 \qquad (24)$$

(crossover frequencies)

$$\frac{15}{1-\Lambda}\,\alpha + \frac{12}{1-4\Lambda}\,\beta = 16 \qquad (25)$$

(cutoff frequencies)

$$15\left[\frac{1+16\Lambda^2}{1-\Lambda^2}\right]\alpha + 12\left[\frac{1+64\Lambda^2}{1-16\Lambda^2}\right]\beta = 16 \qquad (26)$$

(ion-ion hybrid resonances)

$$15\,\alpha + 3\,\beta = 16\,\frac{\Omega^2_{LH}}{\Omega_1\Omega_e}\left[1 + (\Omega_e/\pi_e)^2\right] - 1 \qquad (27)$$

(lower hybrid resonance)

It is easily shown that any two of the above equations can be solved to obtain the relative concentrations (i.e., the determinant of the α, β coefficients is nonzero). A combination

which may be particularly useful is the measurement of the crossover frequency ω_{12} and the lower hybrid resonance Ω_{LH}. As shown in Sections 5 and 6 these critical frequencies have both been observed in satellite VLF data. The solutions for α and β in terms of ω_{12} and Ω_{LH} is shown in Figure 10. Another combination giving a particularly simple relation for α and β is the measurement of the two crossover frequencies $\Lambda_{12} = \omega_{12}/\Omega_1$ and $\Lambda_{23} = \omega_{23}/\Omega_1$. We obtain:

$$\alpha = (16/15)\,(256/255)\,(1 - \Lambda_{12}^2)\,(1 - \Lambda_{23}^2)\,. \tag{28}$$

$$\beta = \frac{16}{225}\,(16\Lambda_{12}^2 - 1)\,(1 - 16\Lambda_{23}^2)\,. \tag{29}$$

These equations are used in Section 5 to estimate the concentration α from proton-whistler data.

The topological shapes of the wave-normal surfaces have been determined for each bounded volume in (Λ, α, β) space. The wave-normal surfaces for the two branches of n^2, labeled according to the L, R scheme, have the four topological configurations sketched in Figure 6. The sketches have been numbered 1 through 4 and the wave-normal surfaces appropriate for each bounded volume are indicated by the corresponding

sketch number. Figure 9 also shows wave-normal surfaces and these are numbered to agree with Figure 6.

It is evident from Figure 6 that at the bounding surfaces only four types of transitions occur, these transitions being repeated for each ion. The transitions at these bounding surfaces have been discussed by Stix [1962] and by Smith and Brice [1964]. These transitions are discussed only briefly here. First, at $L = \infty$ the outer wave-normal surface labeled R suffers no discontinuities due to crossing the bounding surface, and the crossing is an intact transition. The inner wave-normal surface labeled L in sketch 4 suffers a destructive transition when the vertex angle θ_R for the dumbbell lemniscoid goes to zero as $L = \infty$ is approached from the left. Since the wave-normal surface labeled L is profoundly influenced by the ion cyclotron resonance at $L = \infty$, Stix [1962] chose to call this wave an ion cyclotron wave. For frequencies much less than the ion gyrofrequencies this left-hand polarized wave is the slow (shear) hydromagnetic wave first treated by Alfven. Here, we call the ion cyclotron wave just below the proton gyrofrequency a proton cyclotron wave, the ion cyclotron wave just below the He^+ gyrofrequency a He^+ cyclotron wave, etc. Stix shows that

if $K_\perp$ is held constant then $K_\parallel$ approaches infinity as the ion cyclotron resonance is approached; thus, the ion cyclotron wave is refracted toward the surface where $\Omega_K = \omega$ and the ion cyclotron resonance takes place at $\theta = 0$.

The second type of transition evident in Figure 6 occurs at each hybrid resonance $S = 0$, separating regions having wave-normal surfaces labeled R and shown in sketches 1 and 2. It is evident from the refractive index for the transverse X-wave that the phase velocity at $\pi/2$ goes to zero as the bounding surface $S = 0$ is approached. As the surface $S = 0$ is crossed from left to right the topological sphere in sketch 1 deforms continuously into a dumbbell lemniscoid. The transition at $S = 0$ is a reshaping transition.

The third type of transition occurs at each cutoff surface $L = 0$. Cutoffs separate regions having wave-normal surfaces shown in sketches 2 and 3. In sketch 3 the inner surface labeled R is a dumbbell lemniscoid and suffers no discontinuities due to crossing a bounding surface $L = 0$. The outer surface labeled L is a topological sphere. As the bounding surface $L = 0$ is approached from the right the refractive index goes to zero

for all angles and the real wave-normal surface labeled L transforms into an imaginary surface at $L = 0$. Thus the wave-normal surface labeled L suffers a destructive transition at the bounding surface $L = 0$.

The fourth type of transition occurs at the bounding surface $D = 0$ and separates regions having wave-normal surfaces shown in sketches 3 and 4. In the neighborhood of $D = 0$ both the plus and minus branches of n^2 have real wave-normal surfaces. The outer (fast) wave-normal surface, a topological sphere, corresponds to the plus branch of n^2. The inner (slow) wave-normal surface, a dumbbell lemniscoid, corresponds to the minus branch of n^2. As the surface $D = 0$ is crossed the wave-normal surfaces for the two branches both change in a continuous fashion and suffer no discontinuities due to the crossing. Therefore, the transition at the surface $D = 0$ is an intact transition for both branches of n^2. At the surface $D = 0$ it can be verified from Eq. (12) that the fast mode is isotropic and that the wave-normal surfaces are tangent at $\theta = 0$. From the polarization Eq. (16) it is evident that the right (R) and left (L) labels for the fast and slow modes are interchanged at $D = 0$. For the case $\theta = 0$ the wave-polarization ρ is discontinuous and undefined

at $D = 0$. For all angles $\theta \neq 0$ the wave-polarization for the slow mode approaches zero in a continuous fashion as $D = 0$ is approached. At $D = 0$ the wave-polarization for the slow mode is zero ($\rho_- = 0$), so we have

$$E'_{y'} = \rho \; E'_{x'} = 0$$

$$\text{for} \quad D = 0 \quad \text{and}$$

$$\theta \neq 0 \; .$$

Thus the electric vector for the slow mode is linearly polarized in the $(\vec{K}, \vec{B})$ plane for all angles $\theta \neq 0$. The wave-polarization for the fast (isotropic) mode at $D = 0$ is undefined using Eq. (16) since $Sn^2 - RL = 0$ and $D = 0$. Hence, the homogeneous field Eq. (1) must be investigated to determine the fields. With $n^2 = R = L$ Eq. (1) becomes:

$$\begin{bmatrix} R \sin^2 \theta, & P \sin \theta \cos \theta \\ R \sin \theta \cos \theta, & P - R \sin^2 \theta \end{bmatrix} \begin{bmatrix} E_X \\ E_Z \end{bmatrix} = 0$$

$$E_Y = \text{anything}$$

(30)

Equation (30) has no nontrivial solutions ($\theta \neq 0$) for E_X and E_Y unless P = R. This condition is never satisfied in the case considered here so $E_X = E_Z = 0$. Thus the electric field for the fast wave at D = 0 ($\theta \neq 0$) is linearly polarized in the direction normal to the $(\vec{K}, \vec{B})$ plane and perpendicular to the electric field of the slow wave at D = 0. The results just presented concerning the wave-polarization at D = 0 hold only for a collisionless plasma. In the next section we find that collisions strongly influence the wave-polarization in the vicinity of D = 0.

In Figure 6 the refractive index squared for the longitudinal and transverse waves has been plotted in dashed and solid lines. As the parameter Λ is changed the solid lines follow the refractive index at $\theta = 0$ and $\pi/2$ for the wave-normal surface which deforms in a continuous manner at the bounding surfaces. The dashed lines have the same significance. It is evident that the fast and slow wave-normal surfaces touch only at the points where both D = 0 and $\theta = 0$, and that the accessibility of various points in (Λ, α, β) space, via a given continuously deformable wave-normal surface, is limited by cutoffs and resonances. In the next section we find that coupling between

the two modes of propagation near $(D = 0, \theta = 0)$ can extend the region of accessibility in the (Λ, α, β) space.

(4.2) The Critical Coupling Condition.

The differential equations which describe the propagation of a plane wave in a horizontally stratified ionosphere may be written as a set of four simultaneous linear differential equations [Budden, 1961]. Such a system of equations, in general, has four independent solutions. This system of equations is said to be written in coupled form if the dependent variable having the highest order derivative is different for each equation, and the number of dependent variables is equal to the number of equations.

In a given equation the terms in the dependent variable having the highest order derivative are called the principal terms and the remaining terms are called coupling terms. It often happens that if the parameters of the medium vary slowly with altitude, the coupling terms may be neglected for some range of altitudes. Under these conditions the equations become four separate equations which may be solved approximately using the W.K.B. method. In using the W.K.B. method one solves for

the waves in a homogeneous medium having the same parameters as the actual ionosphere at some given altitude. In general four solutions of the form $\exp\left[i\left(\vec{K}\cdot\vec{r} - \omega t\right)\right]$ are obtained, two upgoing waves of opposite polarization and two downgoing waves of opposite polarization. These solutions are called characteristic waves. Approximate W.K.B. solutions resembling the four characteristic waves can be constructed if the dispersion relation $K(\omega)$ is known for all altitudes and directions of propagation.

The method of characteristic waves fails at levels for which the coupling terms are not small. Försterling [1942] derived the following second order coupled equations for vertical incidence. The derivation uses the result that $\rho_o\rho_x = 1$, mentioned in Section 3.2.

$$F_o'' + F_o\left(n_o^2 + \psi^2\right) = \psi' F_x + 2\psi F_x' \tag{31}$$

$$F_x'' + F_x\left(n_x^2 + \psi^2\right) = \psi' F_o + 2\psi F_o'$$

$$\psi = \frac{1}{2K}\frac{d\rho_o}{dZ}\frac{1}{\left(\rho_o^2 - 1\right)} = \frac{1}{2K}\frac{d}{dZ}\log\frac{\rho_o - 1}{\rho_o + 1} \tag{32}$$

The dependent variables F_o and F_x are proportional to the electric fields for the two modes of propagation, here called ordinary (o) and extraordinary (x). The variable ψ which serves to couple the two equations is called the coupling parameter and is a function of the wave-polarization ρ. If the coupling parameter ψ is negligibly small, as it would be in a homogeneous medium where ρ is constant, Eq. (31) shows that the ordinary and extraordinary waves propagate independently. When $\rho = \pm 1$ the coupling parameter is infinite if $d\rho/dZ$ is finite. This condition is called critical coupling and the ordinary and extraordinary waves are strongly coupled in regions near $\rho = \pm 1$. Clemmow and Heading [1954] have formulated the coupled equations for the general case of oblique incidence. [Also see Budden, 1961.] At VLF frequencies it is often sufficient to consider only vertical incidence in the lower ionosphere since a wave incident on the ionosphere from below is refracted to nearly vertical incidence upon entering the ionosphere.

The W.K.B. approximation is valid whenever the relative change in the refractive index per wavelength in the medium is small. This condition may be written [Allis, 1963]:

$$\frac{1}{n^2}\,\frac{dn}{dZ}\,\frac{c}{\omega} << 1 \,. \qquad (33)$$

This condition is clearly violated near altitudes where $n = 0$. This situation also arises when one considers the coupled wave equations. At altitudes where $n \tilde{=} 0$ or dn/dZ is large there is strong coupling between upgoing and downgoing waves [see Clemmow and Heading, 1954]. Physically this corresponds to reflection at any altitude where $n = 0$.

Since the wave polarization is always imaginary for a collisionless plasma, we conclude that the critical coupling condition $\rho_o = \rho_x = \pm 1$ cannot occur except for cases where ρ is undefined: $(\theta = 0,\ D = 0)$, $(\theta = \pi/2,\ n_x^2 = P)$. Therefore, we consider a plasma having collisions. For a plasma having collisions the quantities R, L, P, etc., become complex quantities when m_K is replaced by $m_K (1 + iZ_K)$. These quantities will be written as the sum of their real and imaginary parts, $R = R_o + iR_1$, etc. If Eqs. (5), (6), (7), and (8) are expanded to first order in the parameters Z_K, it is evident that the real part of these equations is the same as for the collisionless case. Then the surfaces $L_o = 0$, $D_o = 0$, etc., are the same as those discussed in Section (4.1).

The critical coupling condition for a plasma having collisions can be stated in terms of the refractive index as follows, from Eq. (16):

$$n^2 = \frac{\rho RL}{\rho S - iD \cos\theta} \quad . \tag{34}$$

It is evident that the critical coupling condition $\rho_x = \rho_o = \pm 1$ implies that $n_x = n_o$, or from Eq. (12)

$$F^2 = H^2 \sin^4 \theta + 4P^2D^2 \cos^2 \theta = 0 \tag{35}$$

where $H = H_o + iH_1 = RL - PS$.

We now assume that the collision frequency is small enough that

$$P_1^2 << P_o^2, \quad R_1^2 << R_o^2, \quad L_1^2 << L_o^2,$$
$$\text{and} \quad H_1^2 << H_o^2 .$$

Omitting the second-order terms in small quantities, the real and imaginary parts of $F^2 = 0$ are:

$$H_o^2 \sin^4 0 + 4P_o^2 \left[D_o^2 - D_1^2 \right] \cos^2 \theta = 0 \tag{36}$$

$$H_1 H_o \sin^4 \theta + 4P_o^2 D_1 D_o \cos^2 \theta = 0 . \tag{37}$$

Equation (36) has a solution if and only if $-D_1 \leq D_o \leq D_1$. Since D_1 is a small quantity $D_1^2 << R_o^2 + L_o^2$, we see that critical coupling can occur only in the immediate neighborhood of the bounding surface $D_o = 0$. Equations (36) and (37) can be solved for the critical coupling angle θ_c and for a critical coupling surface in parameter space.

$$\sin^2 \theta_c \tan^2 \theta_c = \frac{-4P_o^2 D_1 D_o}{H_1 H_o} \tag{38}$$

$$\frac{D_1}{D_o} - \frac{D_o}{D_1} + \frac{H_o}{H_1} = g(\alpha, \beta, Z_K, \Lambda) = 0. \tag{39}$$

Given α, β, Z_K, and Λ as functions of altitude, Eq. (39) can in principle be solved for the critical coupling altitude h_c. This altitude is very close to the altitude where $D = 0$, since $D_o^2 \leq D_1^2 << R_o^2 + L_o^2$. The values of α, β, Z_K, and Λ at altitude h_c can then be substituted into Eq. (38) to give the critical coupling angle θ_c.

Using the assumption that $H_1^2 << H_o^2$, Eq. (39) can be written $D_o/D_1 = H_1/H_o$. Thus D_o can be eliminated from Eq. (38) to give θ_c in terms of quantities which are easily estimated in the vicinity of $D_o = 0$.

$$\sin^2 \theta_c \tan^2 \theta_c = \left. \frac{-4P_o^2 D_1^2}{(R_o L_o - P_o S_o)^2} \right|_{D_o = 0} \tag{40}$$

or $\theta_c^2 \simeq \frac{2|D_1|}{|R_o|}$ if $|R_o| << |P_o|$.

To illustrate the magnitude of the critical coupling angle, consider the $D = 0$ condition illustrated in Figure 9 at $\Lambda = 0.5$, and $\alpha = 0.8$. If we let $Z_1 = Z_2 = 10^{-2}$ then

$\theta_c = 10.7°$. Thus, if collisions had been included, the wave-normal surfaces shown in Figure 9 at D = 0 would intersect for a cone of directions making an angle $\theta_c = 10.7°$ with the magnetic field. This cone will be called the critical coupling cone. Two characteristic waves propagating with $\vec{K}$ near the critical coupling cone are strongly coupled in the vicinity of D = 0.

(4.3) Bounding Surfaces, Accessibility, and Mode Coupling for a Model Ionosphere.

We now consider the propagation of a plane wave in a model ionosphere consisting of a horizontally stratified, neutral mixture of H^+, He^+, O^+ and electrons. The electron and ion density profiles which have been assumed for these calculations are shown in Figure 11 (a). This ionospheric model has been chosen as representative of a mid-latitude ionosphere during local night. The ion density profiles have been sketched using the method by N. Smith [1964]. The equal concentration altitudes and the temperature agree with measurements by Donley [1963], taken during local night. The electron density profile is a qualitative model presented by Bourdeau [1963] for a local time of 02:00. Figure 11 (a) shows that each of the three ionic constituents (H^+, He^+, O^+) predominate in a different altitude region. The thickness of each of these regions is strongly dependent on the ionospheric temperature.

For daytime conditions, the temperature is higher and the equal concentration points move to higher altitudes. In an experimental situation we can expect departures from the model assumed here, since the composition of the ionosphere depends upon local time, latitude, season, etc. An excellent brief report on the composition of the ionosphere has been given by Bourdeau [1963] and references to a large body of experimental work are quoted.

Using the ion density profiles, the critical frequencies (cutoff, resonance, and crossover) have been plotted as a function of altitude in Figure 11 (b). Crossing a critical frequency in this plot corresponds to crossing a bounding surface in the parameter space discussed in Section 4.1. The critical frequencies have been labeled by the corresponding equation for the bounding surface, $L = \infty$, $L = 0$, $S = 0$, and $D = 0$. The resonances labeled $L = \infty$ are the gyrofrequencies for H^+, He^+, and O^+. The critical frequencies labeled $L = 0$, $S = 0$, and $D = 0$ have been obtained from the bounding surface contours in Figures 7 and 8. At each altitude the ion density profiles give values for the relative concentrations α and β. For these values of α and β the roots of $L(\Lambda) = 0$, $S(\Lambda) = 0$, and $D(\Lambda) = 0$ can be found from the bounding surface contours. The critical frequencies are calculated from these roots using $\omega = \Lambda \Omega_1$.

From the discussion in Section 4.1 it is evident that two real wave-normal surfaces exist in the crosshatched region between the cutoffs $L = 0$ and the resonances $L = \infty$. The crosshatched regions below Ω_1, Ω_2, and Ω_3 are the regions of propagation for the proton cyclotron wave, the He^+ cyclotron wave, and the O^+ cyclotron wave, respectively. In the regions not crosshatched, only one real wave-normal surface exists and it is labeled R. It is evident that the predominant concentration of O^+ and He^+ in the lower ionosphere prevents the direct propagation of a lightning impulse to high altitudes entirely via the proton cyclotron mode. It is important to note how the region of propagation for the ion cyclotron mode depends upon the ion concentrations. This dependence on ion concentrations is illustrated in Figures 12 and 13 which show the regions of propagation for the ion cyclotron mode during local night (800° K) and local day (1200° K), respectively. The lower hybrid resonance frequency Eq. (23) is also shown in these figures. The ionospheric model for local day, used to calculate the critical frequencies in Figure 13, is after Anderson and Francis [Walt, 1964]. It is evident that as the ionospheric temperature is increased the equal concentration points move to higher altitudes and the region of propagation for the ion cyclotron waves moves up correspondingly.

We now consider what regions of the ionosphere are accessible to waves from a source having a fixed frequency and located, first, at high altitudes (above 2,500 km), and second, below the base of the ionosphere (200 km). To be specific we consider the frequency 400 c/s. In Figure 11 (c) the phase velocities for 400 c/s are shown as a function of altitude. The dashed lines give the phase velocity at $\theta = 0$ for the fast mode (the outer wave-normal surface between $L = 0$ and $L = \infty$). The wave-normal surface (dashed) for this mode is a topological sphere and deforms in a continuous manner for all altitudes above $L = 0$. Thus, for a source of 400 c/s down-going waves, located at 2,500 km, all altitudes above $L = 0$ are accessible via the mode having the dashed wave-normal surface. At the cutoff $L = 0$, a down-going (fast) wave is reflected since the refractive index goes to zero at this altitude (infinite phase velocity). At the altitude $D = 0$, the wave-polarization changes sign and the label for the fast mode changes from R to L for down-going waves. For the moment, the possibility of mode coupling near $D = 0$ is ignored.

The solid lines in Figure 11 (c) give the phase velocity at $\theta = 0$, 20°, and 30° for the slow mode (the inner wave-normal surface between $L = 0$ and $L = \infty$). The wave-normal surface for

this mode (solid lines) is real for all altitudes below the resonance $L = \infty$, and deforms in a continuous manner over this range of altitudes. Thus, for a source of up-going waves located at the base of the ionosphere all altitudes up to the resonance $L = \infty$ are accessible via the mode having phase velocities shown with solid lines in Figure 11 (c). For an up-going wave ($\theta \neq 0$) starting at the base of the ionosphere, the wave-polarization ρ approaches zero in a continuous manner as the surface $D = 0$ is approached. At $D = 0$ the wave is linearly polarized in the $(\vec{K}, \vec{B})$ plane. As the surface $D = 0$ is crossed the wave-polarization changes sign and the label for the slow wave-normal surface changes from R to L. Proceeding to higher altitudes, the wave propagates via the wave-normal surface labeled L, the proton cyclotron mode. In the next section it is shown that this proton cyclotron wave, between $D = 0$ and $L = \infty$, gives the proton-whistler traces described in Section 2. As the proton cyclotron wave approaches the altitude where the proton gyrofrequency is equal to the wave frequency (400 c/s), the phase velocity approaches zero and the wave energy is absorbed by the plasma.

From the phase velocity plots in Figure 11 (c) and the discussion of wave-normal surfaces in Section 4.1, it is evident

that the wave-normal surfaces shown with solid lines touch but never intersect those shown in dashed lines. The wave-normal surfaces touch at the one point $D = 0$, $\theta = 0$. If we neglect mode coupling and consider the case $D = 0$, $\theta = 0$ to be of measure zero, we must conclude that regions of the ionosphere above $L = \infty$ (for a given frequency) are not accessible to up-going waves starting at the base of the ionosphere. Experimentally it is well known that regions high in the ionosphere, well above $L = \infty$, are accessible to waves having sources below the ionosphere. The observations of multiple hop whistlers having frequencies continuous down to 200 c/s illustrate this point. We conclude that the mode coupling considerations discussed in Section 4.2 are an important aspect of wave propagation in the ionosphere at these frequencies.

Using the equations discussed in Section 4.2, we can consider mode coupling for the special case of vertical incidence by including collisions in the model ionosphere presented in Figure 11. This case is of interest because waves incident on the base of a horizontally stratified ionosphere at angles not too oblique are refracted to nearly vertical incidence in the lower regions of the ionosphere where $n >> 1$. For the frequency 400 c/s in Figure 11 (c), the critical coupling angle at $D = 0$

has been calculated to be $\theta_c = 4.1°$. The collision frequencies at D = 0 were calculated using equations by Nicolet [1953], assuming coulomb collisions. If we assume that the magnetic field is nearly vertical, then for vertical incidence the $\vec{K}$ vector at D = 0 is in a direction near the critical coupling cone and the two modes of propagation are strongly coupled near D = 0. Thus, an upgoing wave originating at the base of the ionosphere generates a second wave of opposite polarization as it passes through the coupling region near D = 0. At altitudes above D = 0 these two waves propagate independently, one following the dashed phase velocity curve labeled R in Figure 11 (c), the other following the solid curve labeled L. The wave following the curve labeled L is an ion cyclotron wave and is absorbed at the resonance $L = \infty$. The other wave-polarization follows the curve labeled R to altitudes well above $L = \infty$. From this example we see that mode coupling has made regions at high altitudes, above $L = \infty$, accessible to waves originating below the ionosphere. If the direction of the magnetic field had been such that $\theta >> \theta_c$ at D = 0, then the coupling would have been much weaker and regions above $L = \infty$ would have been essentially inaccessible.

For many cases of interest the assumption of vertical incidence does not apply and one must consider mode coupling for oblique incidence. The coupled equations for oblique incidence have been investigated by Clemmow and Heading [1954] but have not been considered here. It can be shown,* however, that the critical coupling condition $\rho_o = \rho_x = \pm 1$ continues to apply in the general case and the features illustrated here for vertical incidence will continue to appear.

---

*The coupling coefficient Γ_{ij} for the two upgoing waves is proportional to $(q_i - q_j)^{-1/2}$, where q_i and q_j are the roots of the Booker quartic [see Budden, 1961]. The roots q_i and q_j are equal when $\rho_o = \rho_x = \pm 1$.

5. EVIDENCE THAT PROTON-WHISTLERS ARE ION CYCLOTRON WAVES

In this section we consider the evidence supporting the claim that the proton-whistlers described in Section 2 are ion cyclotron waves.

(5.1) Group Propagation Times for an Impulse Source Below the Ionosphere.

The spectrograms in Figures 1 and 2 give the group propagation time from the source of the lightning impulse to the satellite as a function of frequency. Analytically this may be written as a line integral:

$$\tau(\omega) = \frac{1}{c} \int n_g ds \tag{41}$$

$$n_g = n + \omega \frac{dn}{d\omega} \tag{42}$$

We would like to calculate group propagation times for the model shown in Figure 11 and compare the results with spectrograms of proton-whistlers. Since there is no way of knowing the exact ray path for the whistlers received by Injun III, we must make a reasonable assumption about this path. We assume that along the ray path the $\vec{K}$ vector is always directed approximately along the magnetic field line, that is, we assume quasilongitudinal propagation. For quasilongitudinal propagation the refractive index is approximately $n^2 = R$ or $n^2 = L$, depending whether the wave-normal surface is labeled R or L, respectively.

The group velocity c/n_g for longitudinal propagation ($\theta = 0$) is discontinuous at $D = 0$, where the refractive index changes from $n^2 = R$ to $n^2 = L$. For quasilongitudinal propagation ($\theta \neq 0$) the group velocity changes continuously in the region very near $D = 0$ from that given using $n^2 = R$ to that given using $n^2 = L$. Therefore, for quasilongitudinal propagation we approximate Eq. (41) by using the group refractive index for longitudinal propagation.

The group refractive index for longitudinal propagation is easily calculated from Eqs. (5), (6), and (42), and is given by

$$n\, n_g = 1 - \frac{1}{2} \sum_K \frac{\pm \epsilon_K \pi_K^2 \Omega_K}{\omega(\omega \pm \epsilon_K \Omega_K)^2} \quad . \tag{43}$$

The plus signs apply when $n^2 = R$, and the minus signs apply when $n^2 = L$. If we assume that $n \gg 1$, then $n\, n_g \gg 1$ (since $n_g \geq 1$), and we can omit the 1 on the right side of Eq. (43). With this assumption, and omitting $1 + (\pi_e/\Omega_e)^2$ in Eq. (17) and Eq. (18), the group refractive index can be written in the form: $n_g = \Gamma f(\Lambda,\alpha,\beta)$, where

$$\Gamma^2 = \pi_e{}^2/\Omega_1\Omega_e \quad .$$

The function $f(\Lambda,\alpha,\beta)$ is shown in Figure 14 for $\gamma = 0$ and various values of α. It is evident that n_g is a well-

behaved function for the mode labeled R; whereas for the mode labeled L (the proton cyclotron mode) the group refractive index has an infinity at the proton gyrofrequency ($\Lambda = 1$) and at the cutoff frequency where $L(\Lambda) = 0$. It is instructive to compare this plot of the group refractive index with the C.M.A. diagram for a two-ion plasma in Figure 9.

Group propagation times to various altitudes have been calculated for an impulse source below the ionosphere as a function of frequency. These integrations (Eq. 41) were performed for two cases, both assuming quasilongitudinal propagation and using the model ionosphere in Figure 11 (a). For the first case, it is assumed that mode coupling does not occur. The group propagation time is the sum of the group propagation time via the right-hand polarized mode, plus the group propagation time via the proton cyclotron mode after the polarization reversal at $D = 0$. For these calculations we assume that the wave crosses the $D = 0$ surface between Ω_2 and Ω_3 with no polarization reversal. Thus, we do not consider the He^+ cyclotron wave. Effects because of the He^+ cyclotron wave can occur only below the maximum frequency for which this mode can propagate, about 170 c/s. For the second case, mode coupling was assumed to occur at $D = 0$. Above $D = 0$ two group propagation times must

be calculated; a group propagation time for the right-hand polarized wave generated by the coupling near D = 0, and a group propagation time for the proton cyclotron wave which results from the polarization reversal at D = 0.

The calculated group propagation times are shown in Figure 15 for five altitudes, with and without mode coupling at D = 0. The effect of the infinite group refractive index at Ω_1 for the proton cyclotron wave is clearly evident. For the case without mode coupling the crossover frequency ω_{12} separates the proton cyclotron wave from the right-hand polarized wave. We see that there is a range of frequencies between Ω_1 and Ω_c which do not reach the altitude being considered. The cutoff frequency Ω_c is the maximum frequency along the path for which polarization reversal occurs. Thus, Ω_c is the proton gyrofrequency at the altitude where the bandwidth of the proton cyclotron wave goes to zero, about 690 c/s for the model in Figure 11 (b).

Comparing the delay time curves with the spectrograms of proton-whistlers in Figure 2, we make the following observations:

a. The calculated delay time curves for the proton cyclotron wave are in good quantitative agreement with the proton-whistler traces observed in the Injun III data.

b. The frequency ω_{12}, for which the e-whistler and the proton-whistler are coincident in time, is the crossover frequency at the altitude of the satellite.

c. The dependence of the ratio $\omega_{12}/\Omega_1 = \Lambda_{12}$ on altitude is qualitatively the same for the observed proton-whistlers and the model calculations.

d. The cutoff frequency Ω_c for the e-whistler, observed for some cases in the Injun III data, is the maximum frequency along the path for which polarization reversal can occur.

e. The intensity of the e-whistler trace between Ω_c and ω_{12} is determined by the strength of the coupling near $D = 0$.

These observations suggest that the simple quasilongitudinal propagation model considered here is substantially correct, and that the proton-whistler is a proton cyclotron wave occurring via the polarization reversal at $D = 0$. For a propagation path which is not quasilongitudinal the essential features of the group delay times for upgoing waves are not changed because the polarization reversal condition does not depend upon θ. The propagation path does, however, determine how close $\vec{K}$ is to the critical coupling cone near $D = 0$, and hence determines the intensity of the e-whistler trace between Ω_c and ω_{12}.

If the polarization reversal between Ω_2 and Ω_3 were included, a He^+ cyclotron wave would occur between Ω_2 and ω_{23}, and would be qualitatively similar to the proton-whistler between Ω_1 and ω_{12}. It has been impossible to positively identify any trace in the Injun III data as a He^+ cyclotron wave because of the poor frequency response below 200 c/s.

Because these new whistlers are ion cyclotron waves, we have called them ion cyclotron whistlers. Since an ion cyclotron mode exists for a band of frequencies below each ion gyrofrequency the ion cyclotron whistler traces can be named after the type of ion whost gyrofrequency gives the upper frequency limit of propagation for that wave. Thus, we arrived at the term proton-whistler. Since the right-hand polarized mode can propagate for all frequencies below the electron gyrofrequency we have called the right-hand polarized component of a whistler an electron-whistler.

(5.2) Determining the Relative Concentration α from the Crossover Frequency.

We now consider how proton-whistlers can be used to estimate the concentration parameter $\alpha = n(H^+)/n_e$. A proton-whistler provides two parameters which can be measured with good accuracy. These parameters are the proton gyrofrequency and

the crossover frequency. The proton gyrofrequency is of little interest since it can be calculated with excellent accuracy in the lower ionosphere. The crossover frequency is a function of the parameters α and β, and may be used to obtain information about these parameters. The crossover frequency is the solution of $D(\Lambda,\alpha,\beta) = 0$. Substituting a known value of $\Lambda_{12} = \omega_{12}/\Omega_1$ into this equation gives an equation for α as a function of β. This equation is plotted in Figure 7, and we see that, given Λ_{12}, α is nearly independent of β. Thus, by measuring Λ_{12} the relative concentration $\alpha = n(H^+)/n_e$ at the satellite can be estimated using the contour plot in Figure 7. Equation (28) gives an explicit formula for α as a function of Λ_{12} and Λ_{23}. Since $1/4 > \Lambda_{23} > 1/16$, we can obtain the following inequality for estimating α from the crossover frequency ω_{12}, with ω_{23} unknown.

$$\frac{16}{15}(1 - \Lambda_{12}^2) > \alpha > \frac{256}{255}(1 - \Lambda_{12}^2) .$$

By taking α to be the geometric mean of the right and left hand sides of this inequality α can be estimated to within $\pm$ 3% by measuring ω_{12}.

Using proton-whistlers, α values have been determined for a variety of altitudes during local night (23:00-05:00), and

during local day (11:00-14:00). These α values are presented in Figure 16 and will be compared with existing knowledge of the composition of the ionosphere as further evidence that the explanation of the proton-whistler given here is correct.

The experimental values of α shown in Figure 16 for local night decrease with decreasing altitude, as would be expected from an equilibrium model of the ionosphere. A curve giving α as a function of altitude, for the nighttime model ionosphere used earlier, is shown for comparison with these data. The temperature for the nighttime model ionosphere is 800° K. The agreement between the proton-whistler data and this model is reasonable, although the fractional concentration of H^+ is somewhat larger than that used in the model.

The experimental α values obtained during local daytime are shown in Figure 16. The daytime α values are compared with the daytime model ionosphere used earlier. Again the α values are somewhat larger than those given by the model. By comparing the daytime and nighttime data we see that α values of about 0.6 occur at higher altitudes during the local day (about 1300 km), than during the local night (about 700 km). This diurnal variation is as would be expected since the equal concentration points for the local day are at higher altitudes than those for

local night. The experimental fact that proton-whistlers are observed at lowef altitudes and more frequently during local night than during local day (see Figure 4) is also in agreement with the expected diurnal variation of the bounding surfaces in Figures 12 and 13.

The occurrence of proton-whistlers in latitude is shown in Figure 5. It seems likely that the cut-off at high latitudes (above 55° latitude) may be due in part to the increased plasma temperature near the auroral zone and the resultant higher altitudes of the helium and oxygen ion layers.

6. OTHER RELATED VLF PHENOMENA OBSERVED WITH INJUN III

In this section other VLF phenomena related to the presence of ions in the ionosphere are considered. The phenomena discussed below are known as radio noise emissions and are distinctly different from the proton-whistlers discussed earlier. In contrast to the proton-whistlers, whose source of energy is a lightning impulse, the detailed mechanism via which radio noise emissions are generated in the ionosphere is largely unknown. These radio noise emissions do, however, propagate in the same manner as whistlers and the theory of propagation in multi-component plasmas may be very useful in the study of these radio noise phenomena.

(6.1) Radio Noise Emissions Near the Lower Hybrid Resonance Frequency.

In the VLF recordings from the Alouette I satellite, which used a dipole antenna, an unusual band of VLF radio noise has been reported by Barrington and Belrose [1963]. This noise band has a sharp lower frequency cut-off which usually decreases in frequency with increasing latitude of the satellite. Brice and Smith [1964] have suggested that this noise band is related to the lower hybrid resonance for the ambient plasma Eq. (23). The decreasing lower cut-off frequency with increasing latitude

is thought to be due to systematic changes in the electron plasma frequency and the relative ion concentrations with latitude. Following Brice [1964] we will call this noise band a lower hybrid emission. At the time of this writing no completely satisfactory theory has been published which explains how this noise is generated.

During the first few weeks after Injun III was launched there were three passes for which noise emissions of the type described by Barrington and Belrose were clearly observed in the Injun III VLF recordings. [These observations were reported at the Spring URSI Meeting, April, 1963.] One of these three cases is shown in Figure 14. This spectrogram shows a noise band having a sharp lower frequency cut-off which decreases in frequency with increasing latitude of the satellite, as found in the Alouette data. The magnetic field intensity of the noise band, as detected by the Injun III loop antenna, is about 8.0×10^{-9} gamma^2/cps. This amplitude is about 20 db above the receiver noise level and comparable to the intensity of other VLF phenomena detected by Injun III. The other two examples are similar to the case described above. The coordinates of the Injun III satellite for each of the three passes having lower hybrid emissions are given below:

	UT	LT	Altitude	L	Lower Cut-Off Frequency
(a)	Dec. 18, 1962				
	From 21:29:32	09:50	1232 km	2.59	8.8 kc/s
	To 21:32:37	10:37	1019 km	3.97	4.5 kc/s
(b)	Dec. 19, 1962				
	From 14:51:03	08:58	1582 km	2.92	7.0 kc/s
	To 14:53:01	09:10	1447 km	3.70	4.5 kc/s
(c)	Dec. 21, 1962				
	From 15:18:03	08:32	1567 km	2.56	8.8 kc/s
	15:20:12	08:47	1417 km	3.3	5.5 kc/s

For times preceding and following the above cases there were passes through similar latitude, altitude, and local time coordinates for which no lower hybrid emissions were observed. Thus, certain unknown conditions must be satisfied for the lower hybrid emissions to occur.

After analyzing all the Injun III VLF data from December 15, 1962 to June 15, 1963, no further examples of the lower hybrid emission have been found even though the phenomenon has been found on roughly 60% of the Alouette recordings during this same period [Brice, 1964]. Since the examples observed in the first few weeks after launch were relatively intense this sudden decline in the occurrence of lower hybrid emissions in the Injun III data seems remarkable. As a possible explanation we suggest that the magnetic component of the wave associated with the lower hybrid emission is directed along the geomagnetic field and that the VLF loop antenna on Injun III was relatively insensitive to this phenomenon after the satellite achieved magnetic

orientation. Injun III is oriented by a permanent magnet in the satellite such that the geomagnetic field $\vec{B}_o$ is in the plane of the loop antenna. Shortly after launch the satellite was tumbling and the plane of the loop was typically at a large angle with respect to the geomagnetic field. After approximately three weeks in orbit (January 4, 1963) orientation had been achieved and the angle between the plane of the loop antenna and the geomagnetic field was typically less than about 5°. For this final steady state orientation the loop antenna is relatively insensitive to a wave field whose magnetic component is along the geomagnetic field. For instance, if the angle between the plane of the loop and the geomagnetic field is 5° then the sensitivity of the loop antenna is decreased by about 20 db from the value expected for a random antenna orientation. Thus, the absence of the lower hybrid emission in the Injun III VLF data after December 21, 1962 may be explained by hypothesizing that the magnetic component of the wave field associated with the lower hybrid emission is along the geomagnetic field. This implies that the wave is propagating nearly transverse to the geomagnetic field since we must have $\vec{K} \cdot \vec{B_1} = 0$. This conclusion fits in well with Brice and Smith's hypothesis that the noise is somehow associated with a resonance for propagation transverse to the magnetic field.

In future experiments it is suggested that if one could simultaenously measure the crossover frequency ω_{12} from proton-whistler traces, the lower frequency cut-off of the lower hybrid emission, and the electron density, then the relationships shown in Figure 10 could be used to provide additional evidence that the cut-off frequency of the lower hybrid emission is in fact Ω_{LH}. Alternatively, one could assume that this cut-off frequency is Ω_{LH} and use Figure 10 to estimate the relative concentrations α and β at the satellite. However, until the lower hybrid emissions are understood theoretically it must be assumed that ion concentrations calculated in this manner may not be typical since it appears that certain unknown conditions are required for the lower hybrid emissions to occur.

(6.2) Radio Noise Emissions at Frequencies below 1 kc/s.

Radio noise emissions at frequencies less than 1 kc/s are commonly found in the Injun III VLF data, especially at higher latitudes. Even considering the poor response of the VLF receiver at these frequencies [Gurnett, 1963], radio noise emissions have been found in the Injun III recordings with frequencies as low as 150 c/s. Radio noise emissions in this

frequency range have been observed on the ground by Aarons [1956, 1960], Gustafsson [1960], Egeland [1962], and others. Since the frequencies of these radio noise emissions are on the order of the ion gyrofrequencies, the propagation theory considered here may be particularly relevant to the study of these VLF emission phenomena.

Figure 18 shows two spectrograms of VLF radio noise emissions occurring at frequencies below 1 kc/s. These spectrograms illustrate two features which have been consistently found on spectrograms of radio noise in this frequency range. First, the ratio noise occurring at about 1 kc/s often has a lower frequency cut-off near the proton gyrofrequency Ω_1. Second, well below the proton gyrofrequency another noise band appears and this noise band often has a lower frequency cut-off near the He^+ gyrofrequency Ω_2. At the present time the study of these noise bands is in a very preliminary state and it is not possible to say whether the observed cut-offs are directly related to the ion gyrofrequencies at the satellite or possibly to a cut-off effect similar to the frequency Ω_c observed in the proton-whistler data.

We offer the following comments concerning the noise bands shown in Figure 18. If we assume that the lower frequency cut-off

for the band just above Ω_1 is a propagation effect and not a source characteristic then the wave must be a downgoing wave since the H^+ concentration at, or below, the satellite altitude of about 600 km (Figure 18 (b)) is almost entirely negligible. From the bounding surfaces for the model ionosphere shown in Figure 11 (b) and the discussion in Section 4.3 we note that down-going right-hand polarized waves from a noise source located at high altitudes (above 2,500 km) cannot reach 600 km for any frequency below Ω_c because downgoing waves are reflected at L = 0. We assume that $\vec{K}$ makes a large angle with $\vec{B}$ at D = 0 so that no mode coupling occurs. This model may explain the observed lower frequency cut-off near the proton gyrofrequency.

By placing the noise source at an appropriate altitude this model may also explain the noise band occurring well below Ω_1 and having a lower frequency cut-off near the He^+ gyrofrequency. These comments are quite tentative and a complete study of the experimental data will be necessary before these radio noise emissions can be understood. It is, however, evident that the accessibility considerations discussed in Section 4 may be very relevant to the study of radio noise emissions from the ionosphere at frequencies below 1 kc/s.

7. CONCLUSION

In this paper an experimental study of the proton-whistler was presented and an explanation of this new effect given. It was proposed that the proton-whistler is simply a dispersed form of the original lightning impulse and that the dispersion can be explained by considering the effects of ions on the propagation of an electromagnetic wave in the ionosphere.

A model ionosphere consisting of three ions (H^+, He^+, and O^+) was introduced, and a physically reasonable ion density profile was assumed. For this model the propagation of waves having frequencies on the order of the ion gyrofrequencies was investigated. It was found that for a band of frequencies below each ion gyrofrequency a left-hand polarized wave can propagate. These waves have been called the proton cyclotron wave, the He^+ cyclotron wave and the O^+ cyclotron wave, corresponding to the type of ion whose gyrofrequency provides the upper frequency limit for each band. This nomenclature follows that of Stix, who called all of these waves ion cyclotron waves. The bandwidths of the ion cyclotron waves depend on the relative concentrations of the ions. Because the bandwidths depend on the ion concentrations, the ion cyclotron wave can propagate only for certain ranges of frequencies and altitudes in the ionosphere. The proton-whistler was interpreted as a proton cyclotron wave.

In the ionosphere it was found that, at an altitude determined by the equation D = 0, an upgoing right-hand polarized wave changes polarization and becomes an ion cyclotron wave. Polarization reversal appeared as a crucial feature in the explanation of the proton-whistler because, as was shown, the predominance of O^+ and He^+ in the lower ionosphere prevents the direct propagation of a lightning impulse to the satellite entirely via the proton cyclotron mode.

An investigation of mode coupling for the special case of vertical incidence showed that if collisions are included the condition D = 0 plays an important part in mode coupling theory. It was found that for a small cone of directions around $\vec{B}$, and at an altitude very near the polarization reversal altitude (D = 0), the two modes are critically coupled. In the ionosphere, if an upgoing right-hand polarized wave crosses the polarization reversal altitude (D = 0) with $\vec{K}$ near the critical coupling cone a wave of opposite polarization is generated, and above D = 0 there are two waves of opposite polarization, each propagating independently. One of these, the ion cyclotron wave suffers a destructive transition when the wave frequency becomes equal to the ion gyrofrequency. The other wave above D = 0, a right-hand polarized wave, can propagate to considerably higher altitudes.

To show how these results apply to the proton-whistler, the group propagation times to various altitudes were calculated as a function of frequency, assuming an impulse source below the base of the ionosphere. The propagation was assumed to be quasilongitudinal. The calculated delay time curves agreed well with spectrograms of proton-whistlers and strongly suggested that proton-whistlers are ion cyclotron waves. The propagation theory also suggested that a He^+ cyclotron wave could result from a lightning stroke via a process identical to that by which the proton-whistler occurs. If and when such an effect is found, it might very well be called a helium-whistler. Similar effects might even be expected below the O^+ gyrofrequency. Since these new whistlers are ion cyclotron waves, we have called them ion cyclotron whistlers. For frequencies much less than the ion gyrofrequencies these left-hand polarized whistlers are the slow hydromagnetic waves treated by Alfven. The proton-whistler is, therefore, a direct observation of an Alfven wave propagating in the ionosphere.

The theory presented here has provided a method of determining the concentration parameter $\alpha = n(H^+)/n_e$ at the satellite from proton-whistler data. Experimental values of α, determined by using proton-whistler data, were shown to be in reasonable

agreement with present models of the ion concentration in the ionosphere. This application of propagation theory to a multicomponent plasma shows that radio measurements by satellites at ion gyrofrequencies can provide an excellent diagnostic tool for studying the composition of the ionosphere.

REFERENCES

Aarons, J., Low frequency electromagnetic radiation 10-900 cycles per second, J. Geophys. Res., 61, 647-661, 1956.

Aarons, J., G. Gustafsson, and A. Egeland, Correlation of audio-frequency electromagnetic radiation with auroral zone micropulsations, Nature, 185, 148-151, 1960.

Allis, W. P., Waves in a plasma, Sherwood Conf. Contr. Fusion, Gatlinburg, TID 7582, April 1959.

Allis, W. P., S. J. Buchsbaum, and A. Bers, Waves in Anisotropic Plasmas, M.I.T. Press, Cambridge, Massachusetts, 1963.

Auer, P. L., H. Hurwitz, Jr., and R. D. Miller, Collective oscillations in a cold plasma, Phys. Fluids, 1, 501, 1958.

Barrington, R. E., and J. S. Belrose, Preliminary results from the very-low-frequency receiver aboard Canada's Alouette satellite, Nature, 198 (4881), 651-656, May 18, 1963.

Bourdeau, R. E., Rocket and satellite investigations of the ionosphere, Trans. Am. Geophys. Union, 44, 443, 1963.

Brice, N., Discrete very low frequency emissions from the upper atmosphere, SEL 64-088, Radioscience Lab., Stanford Electronics Labs., Stanford University, Stanford, Calif., August 1964.

Brice, N. M., and R. L. Smith, A very-low-frequency plasma resonance, Nature, 203 (4948), 926-927, Aug. 29, 1964.

Buchsbaum, S. J., Resonance in a plasma with two ion species, Phys. Fluids, 3, 418, 1960.

Budden, K. G., Radio Waves in the Ionosphere, Cambridge University Press, Cambridge, England, 1961.

Clemmow, P. C., and J. Heading, Coupled forms of the differential equations governing radio propagation in the ionosphere, Proc. Cambridge Phil. Soc., 50, 319, 1954.

Clemmow, P. C., and R. F. Mullaly, The dependence of the refractive index in magnetoionic theory on the direction of the wave normal, The Physics of the Ionosphere, The Physical Society, London, 340, 1955.

Donley, John L., Experimental evidence for a low ion-transition altitude in the upper nighttime ionosphere, J. Geophys. Res., 68, 2058-2060, 1963.

Egeland, A., S. Olsen, and G. Gustafsson, Noise emissions in the audio frequency range. Final Report Task, 3, Contract No. AF 61 (514) - 1314, 7 March 1962.

Försterling, K., Über die Ausbreitung elektromagnetischer wellen in einem magnetisierten medium bei senkrechter incidenz, Hochfr Elek, 59, 110, 1942.

Gallet, R., The very low-frequency emissions generated in the earth's exosphere, Proc. IRE, 47 (2), 211-231, 1959.

Gintsburg, M. A., Low-frequency waves in multicomponent plasma, Geomagnetism and Aeronomy, 3, 610-614, 1963.

Gurnett, D. A., Very low frequency electromagnetic emissions observed with the O.N.R./S.U.I. satellite Injun III, SUI Report 63-27, State University of Iowa, Iowa City, Iowa, August 1963.

Gustafsson, G., A. Egeland, and J. Aarons, Audio-frequency electromagnetic radiation in the auroral zone, J. Geophys. Res., 65, 2749-2758, 1960.

Hines, C. O., Heavy-ion effects in audio-frequency radio propagation, J. Atmos. Terr. Phys., 11, 36-42, 1957.

Nicolet, M. J., The collision frequency of electrons in the ionosphere, J. Atmos. Terr. Phys., 3, 200-211, 1953.

Smith, Newbern, A simple method of drawing ion-density profiles in an atmosphere in diffusive equilibrium, Paper 4-4-7, 1964 Spring URSI Meeting, Washington, D. C., April 15-18, 1964.

Smith, R. L., et al., An ion gyrofrequency phenomenon observed in satellites, Nature, 204 (4955), 274, Oct. 17, 1964.

Smith, R. L., and Neil Brice, Propagation in multicomponent plasmas, J. Geophys. Res., 69 (23), 1964.

Stix, T. H., The Theory of Plasma Waves, McGraw Hill Book Co., Inc., New York, 1962.

Walt, Martin, The effects of atmospheric collisions on geomagnetically trapped electrons, J. Geophys. Res., 69, 3947-3958, 1964.

Yakimenko, V. L., Oscillations in a cold plasma containing two ion species, Sov. Phys., Tech. Phys., 7 (2), 117-124, 1962.

FIGURE CAPTIONS

Figure 1. Spectrogram Showing a Proton-Whistler and Nomenclature.

Figure 2. Altitude and Local Time Dependence of ω_{12}/Ω_1 for Proton-Whistlers.

Figure 3. Asymptotic Frequency Ω_1 vs B.

Figure 4. The Occurrence of Proton-Whistlers in Altitude-Local Time Space. These Data Include All Latitudes Sampled by the Satellite.

Figure 5. The Occurrence of Proton-Whistlers in Altitude-Latitude Space. These Data Include All Local Times Sampled by the Satellite.

Figure 6. Refractive Index Squared for the R, L, and X Waves, and Wave-Normal Surfaces in Each Bounded Volume ($\alpha = 0.8$, $\beta = 0.15$, $\gamma = 0.05$).

Figure 7. The Bounding Surfaces D = 0 and L = 0 in Parameter Space.

Figure 8. The Bounding Surface S = 0 in Parameter Space.

Figure 9. The Bounding Surfaces for a Two-Ion Plasma (H^+, He^+) and Wave-Normal Surfaces in Each Bounded Volume.

Figure 10. Determining the Relative Concentrations α and β from the Critical Frequencies Ω_{LH} and ω_{12}.

Figure 11. The Bounding Surfaces and Phase Velocities at 400 c/s for a Model Ionosphere.

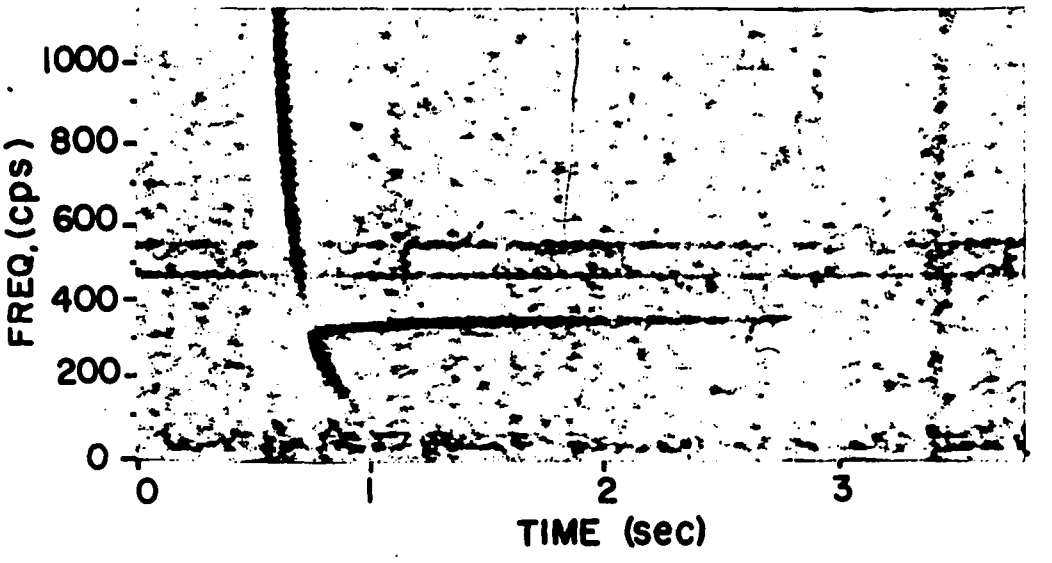

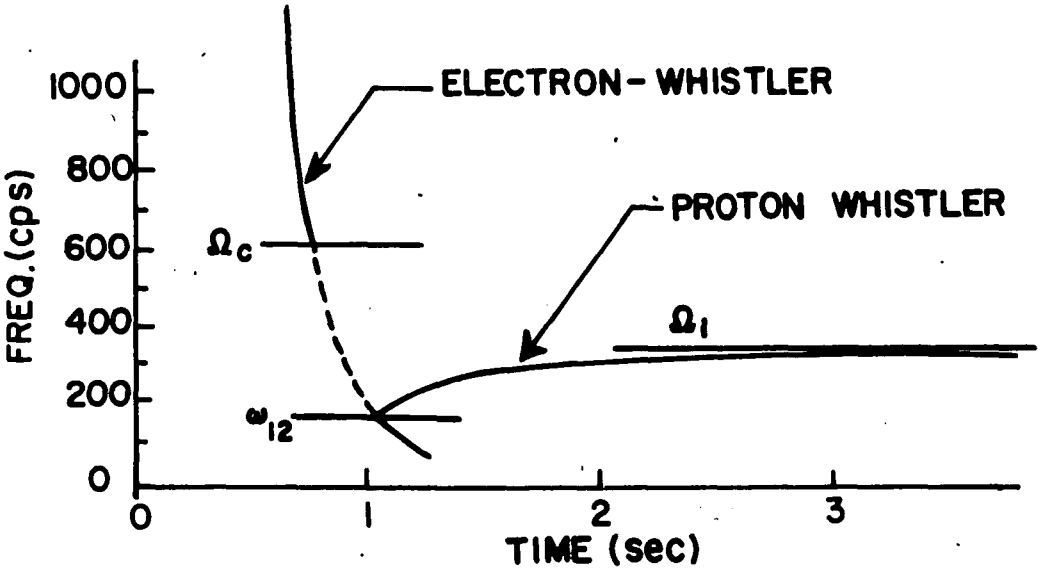

P-WHISTLER SPECTROGRAM AND NOMENCLATURE DIAGRAM

FIGURE 1

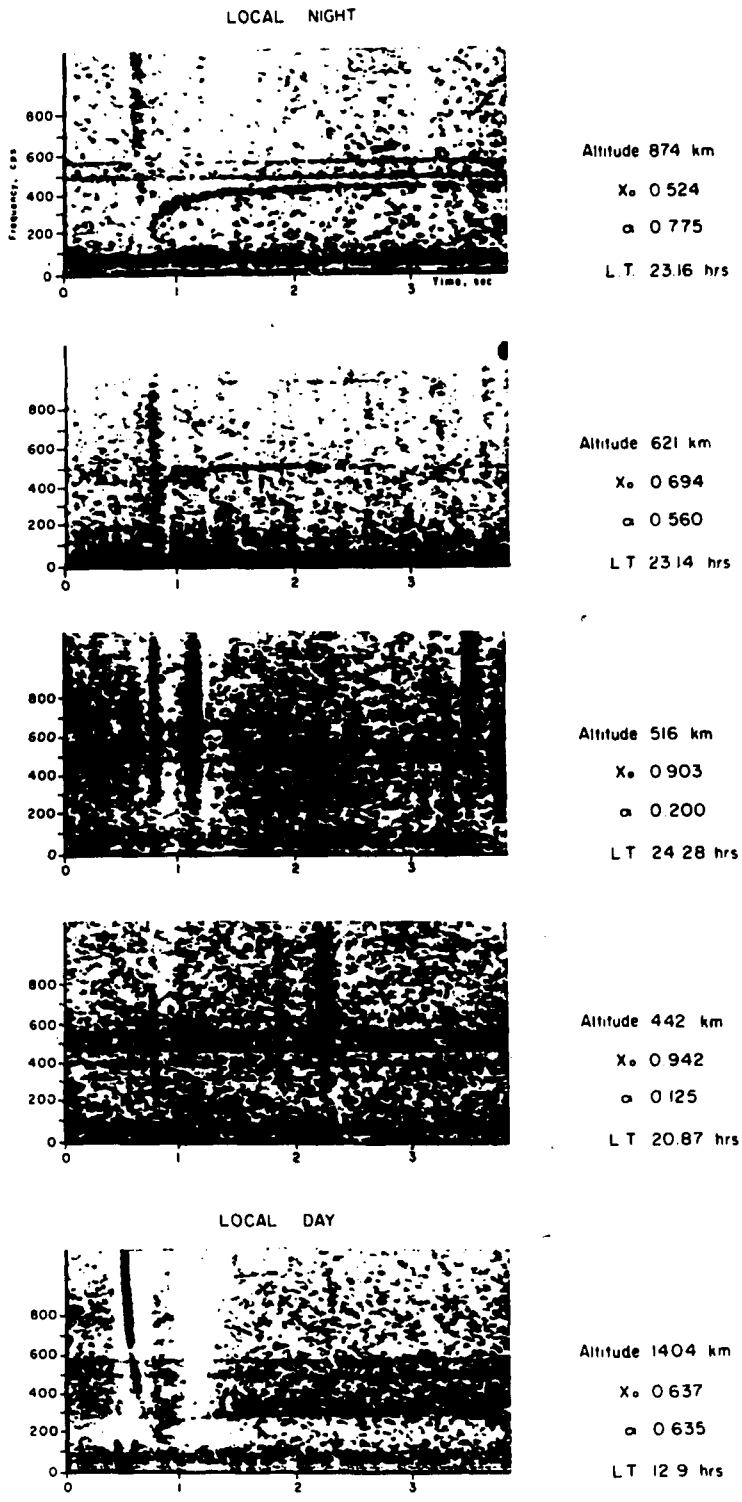
LOCAL NIGHT
Frequency, cps
Time, sec
Altitude 874 km
Xo 0 524
α 0 775
L T 23.16 hrs
Altitude 621 km
Xo 0 694
α 0 560
L T 23 14 hrs
Altitude 516 km
Xo 0 903
α 0 200
L T 24 28 hrs
Altitude 442 km
Xo 0 942
α 0 125
L T 20.87 hrs
LOCAL DAY
Altitude 1404 km
Xo 0 637
α 0 635
L T 12 9 hrs

Figure 2

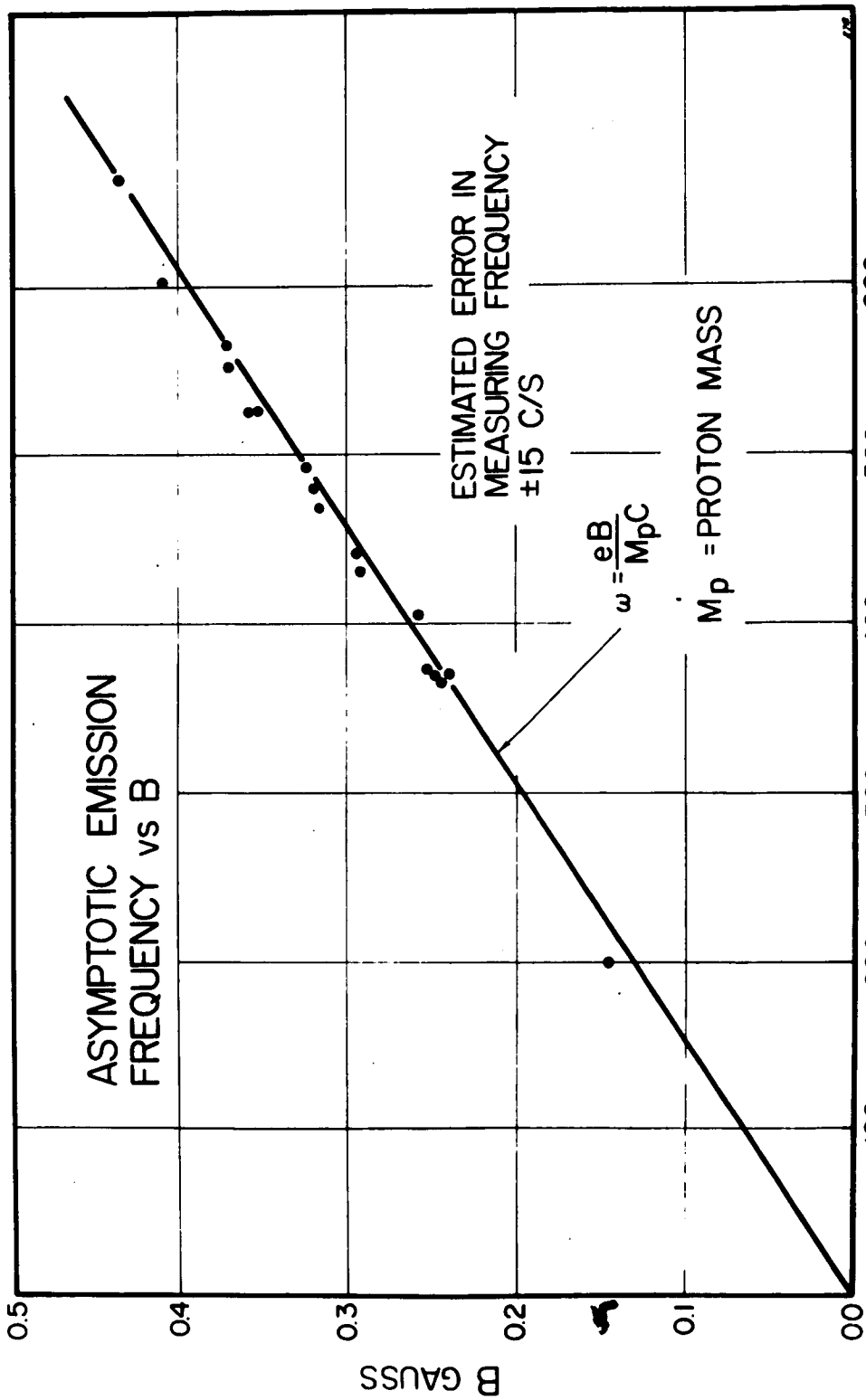
ASYMPTOTIC EMISSION
FREQUENCY vs B
ESTIMATED ERROR IN
MEASURING FREQUENCY
±15 C/S
$\omega = \frac{eB}{M_p C}$
M_p = PROTON MASS
B GAUSS
FREQUENCY C/S
0.0
0.1
0.2
0.3
0.4
0.5
100
200
300
400
500
600

Figure 3

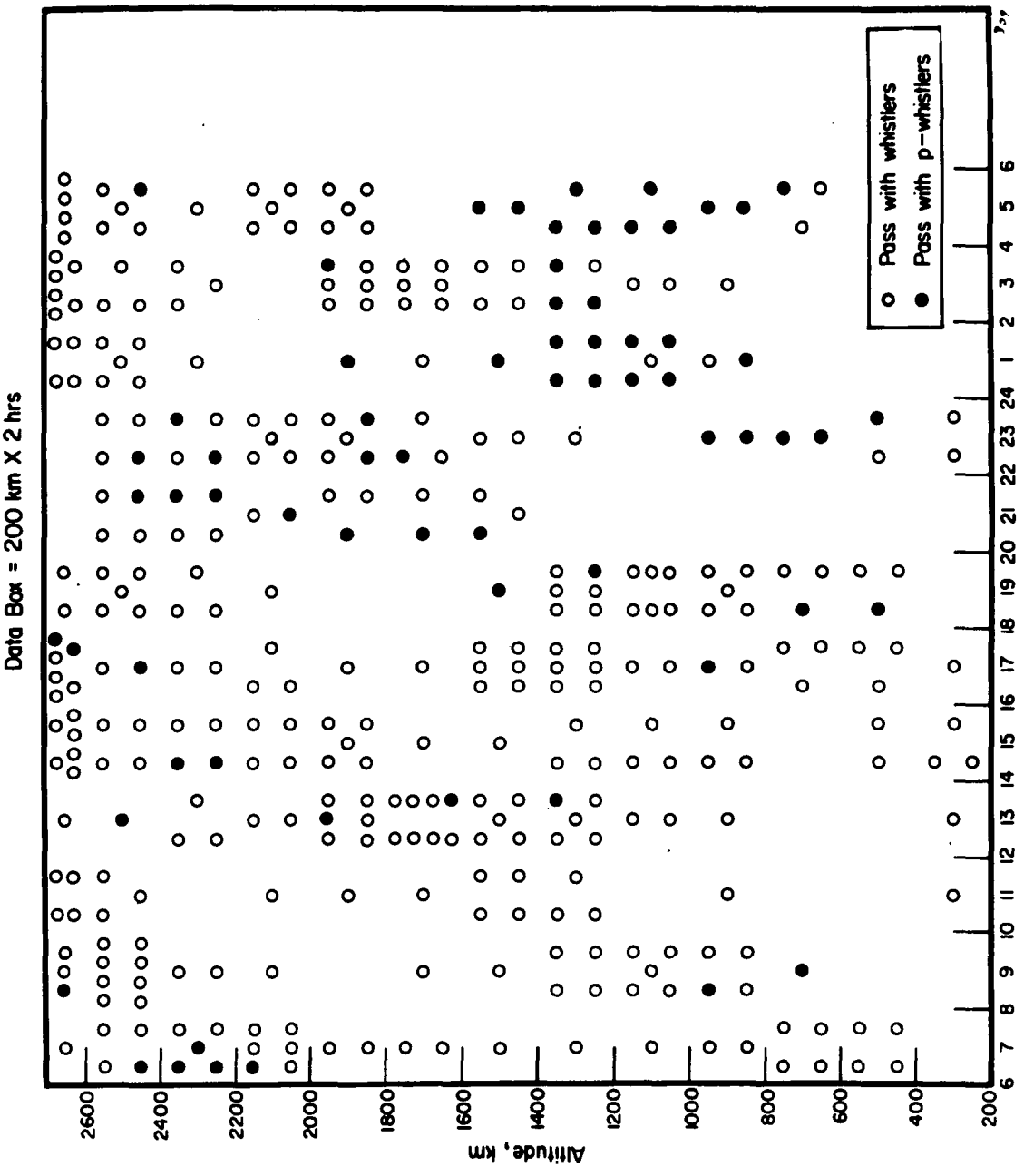
Data Box = 200 km X 2 hrs
Pass with whistlers
Pass with p-whistlers
Altitude, km
Local Time, hrs

Figure 4

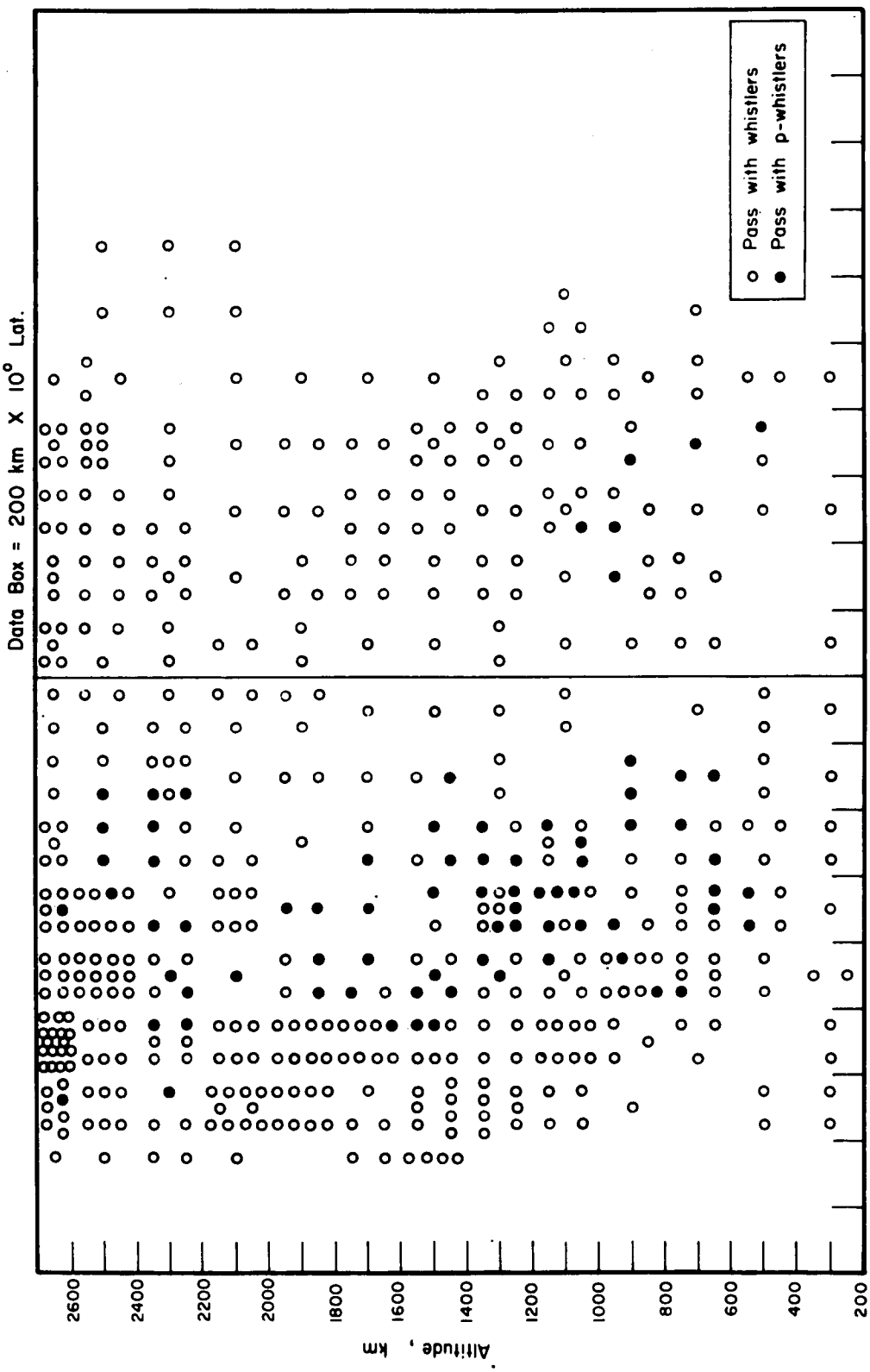
Data Box = 200 km X 10° Lat.
Pass with whistlers
Pass with p-whistlers
Altitude, km
Latitude, degrees

Figure 5

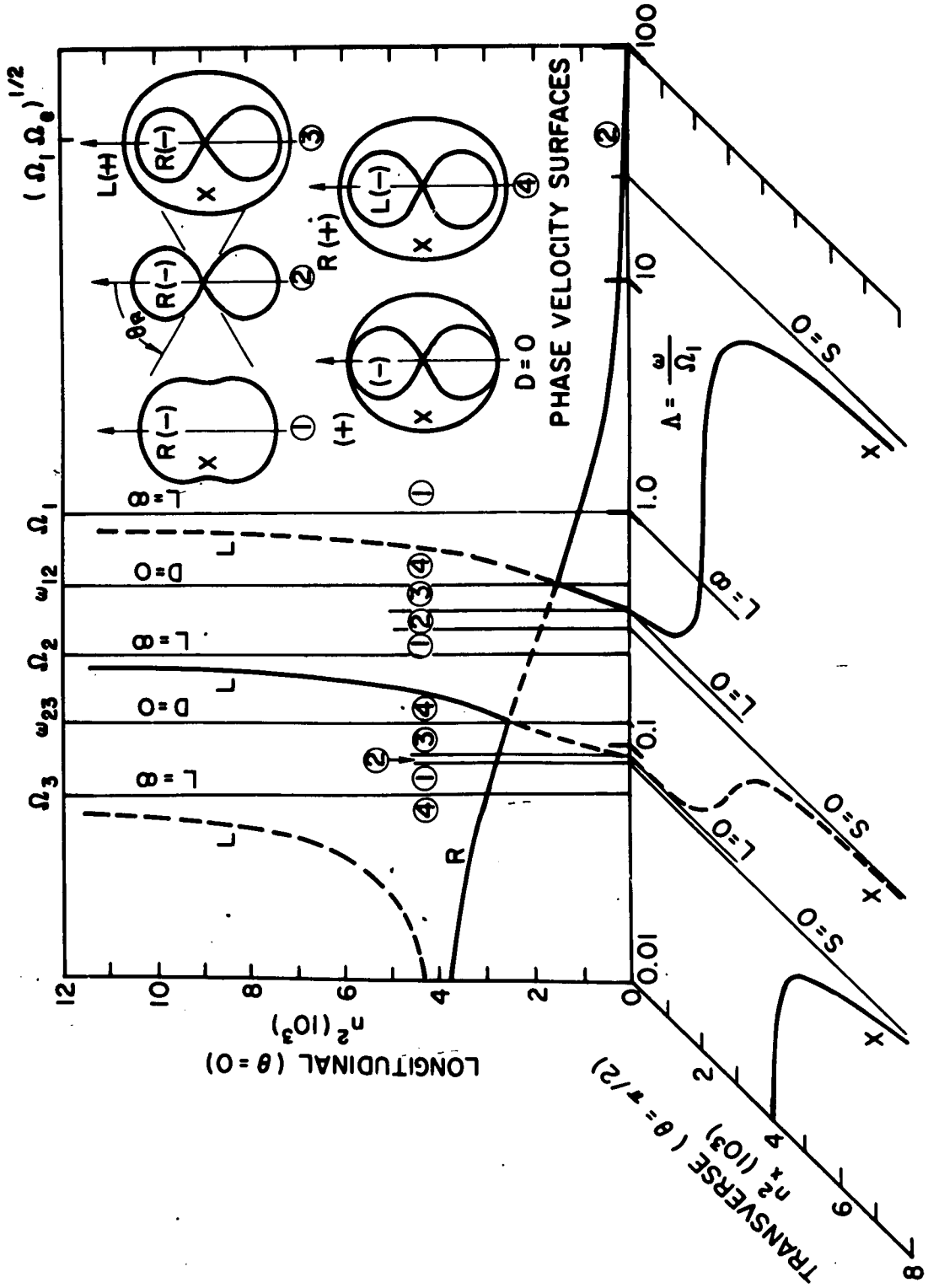
PHASE VELOCITY SURFACES
LONGITUDINAL (θ = 0)
TRANSVERSE (θ = π/2)
n² (10³)
n_x² (10³)
Λ = ω/Ω₁
Ω₁
ω₁₂
Ω₂
ω₂₃
Ω₃
L = ∞
D = 0
R
L
X
S = 0
P = 1
D = 0
L(+)
R(−)
R(+)
L(−)
(+)
(−)
θ_c
(Ω₁ Ω_e)^1/2

FIGURE 6

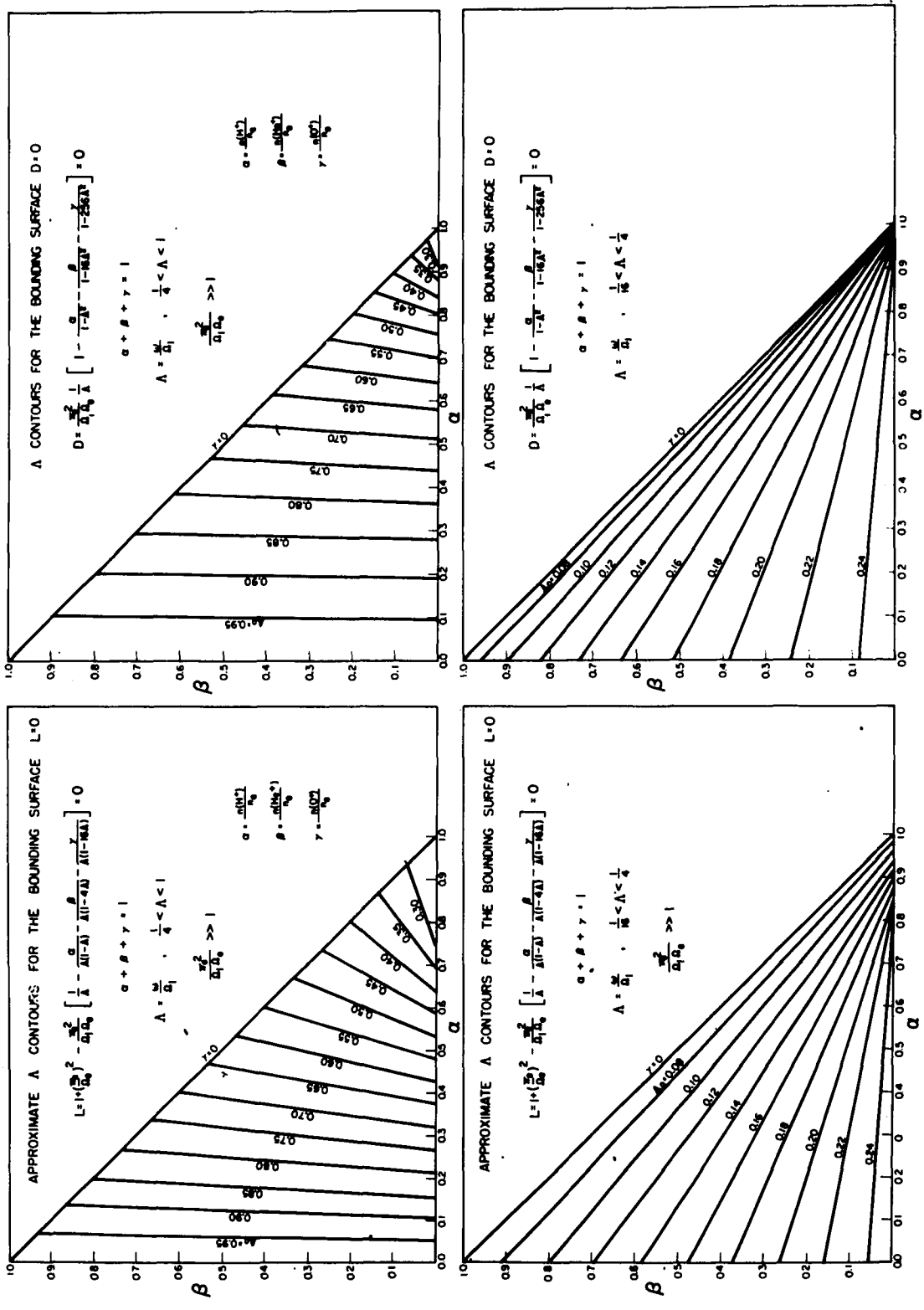
APPROXIMATE A CONTOURS FOR THE BOUNDING SURFACE L=0
Λ CONTOURS FOR THE BOUNDING SURFACE D=0
α
β
α + β + γ = 1
Λ = M/Ω₁ , 1/4 < Λ < 1
π²/Ω₁Ω₀ >> 1
γ=0
Λ=0.95
0.90
0.85
0.80
0.75
0.70
0.65
0.60
0.55
0.50
0.45
0.40
0.35
0.30
0.25
0.20
0.15
0.10
0.05
0.00

FIGURE 7

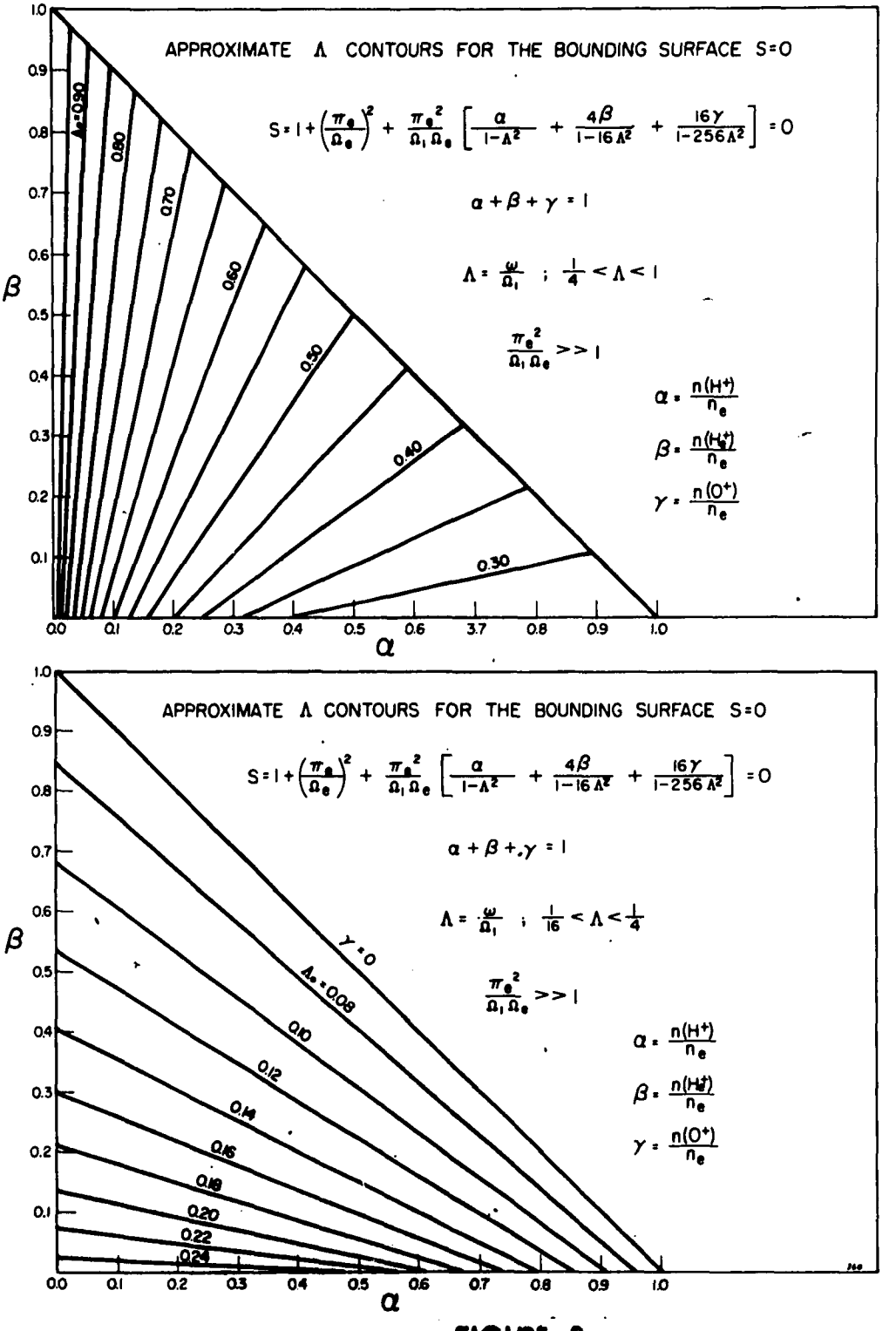
APPROXIMATE Λ CONTOURS FOR THE BOUNDING SURFACE S=0
$S = 1 + \left(\frac{\pi_e}{\Omega_e}\right)^2 + \frac{\pi_e^2}{\Omega_1 \Omega_e}\left[\frac{\alpha}{1-\Lambda^2} + \frac{4\beta}{1-16\Lambda^2} + \frac{16\gamma}{1-256\Lambda^2}\right] = 0$
$\alpha + \beta + \gamma = 1$
$\Lambda = \frac{\omega}{\Omega_1}$; $\frac{1}{4} < \Lambda < 1$
$\frac{\pi_e^2}{\Omega_1 \Omega_e} >> 1$
$\alpha = \frac{n(H^+)}{n_e}$
$\beta = \frac{n(H_e^+)}{n_e}$
$\gamma = \frac{n(O^+)}{n_e}$
Λ_e=0.90
0.80
0.70
0.60
0.50
0.40
0.30
β
α
APPROXIMATE Λ CONTOURS FOR THE BOUNDING SURFACE S=0
$S = 1 + \left(\frac{\pi_e}{\Omega_e}\right)^2 + \frac{\pi_e^2}{\Omega_1 \Omega_e}\left[\frac{\alpha}{1-\Lambda^2} + \frac{4\beta}{1-16\Lambda^2} + \frac{16\gamma}{1-256\Lambda^2}\right] = 0$
$\alpha + \beta + \gamma = 1$
$\Lambda = \frac{\omega}{\Omega_1}$; $\frac{1}{16} < \Lambda < \frac{1}{4}$
$\frac{\pi_e^2}{\Omega_1 \Omega_e} >> 1$
$\alpha = \frac{n(H^+)}{n_e}$
$\beta = \frac{n(H_e^+)}{n_e}$
$\gamma = \frac{n(O^+)}{n_e}$
γ=0
Λ_e=0.08
0.10
0.12
0.14
0.16
0.18
0.20
0.22
0.24
β
α

FIGURE 8

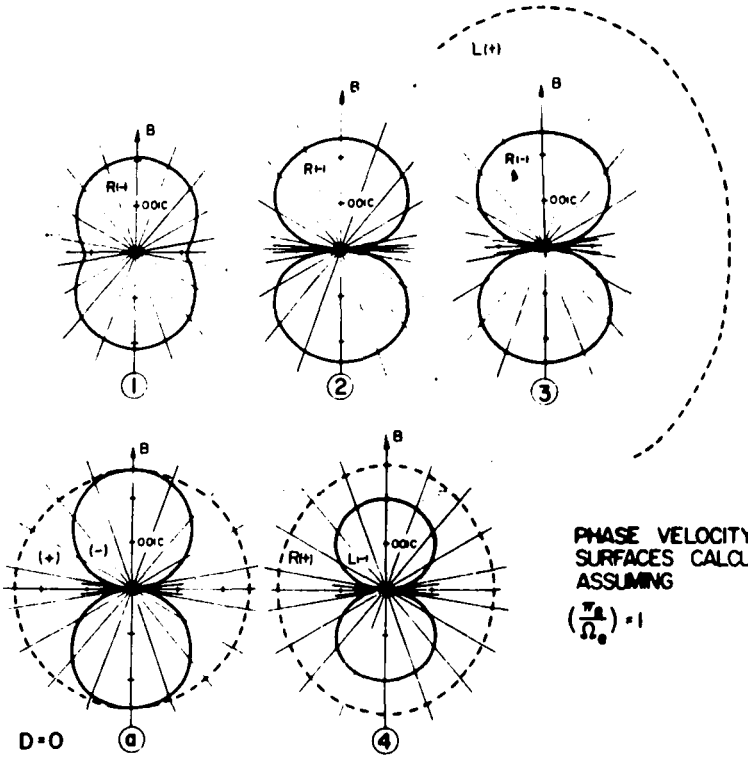
L(+)
B
R(+)
0.01C
1
2
3
(+)
(-)
L(-)
D=0
a
4
PHASE VELOCITY
SURFACES CALCULATED
ASSUMING
$(\frac{\pi_e}{\Omega_e}) = 1$

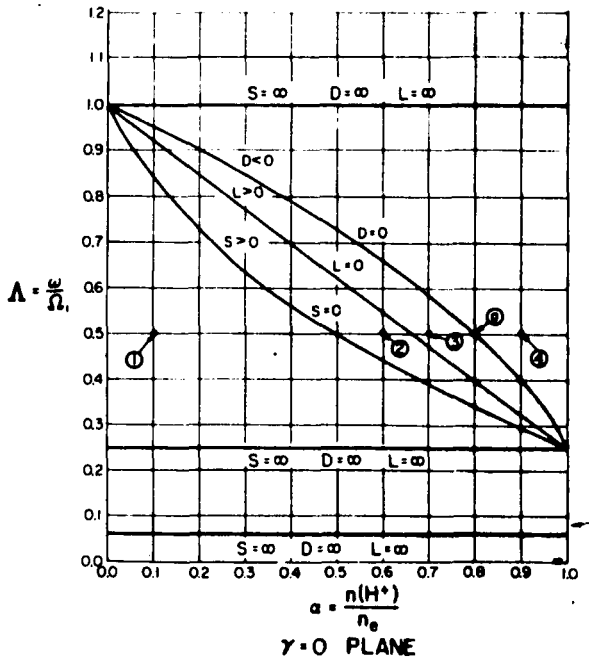
S=∞ D=∞ L=∞
D<0
L>0
S>0
D=0
L=0
S=0
$\Lambda = \frac{\omega}{\Omega_i}$
$\alpha = \frac{n(H^+)}{n_e}$
γ=0 PLANE

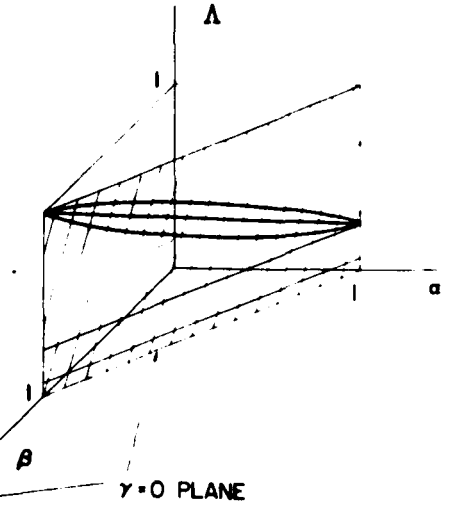
Λ
α
β
γ=0 PLANE

Figure 9

DETERMINING CONCENTRATIONS FROM THE CROSSOVER AND LOWER HYBRID RESONANCE FREQUENCIES

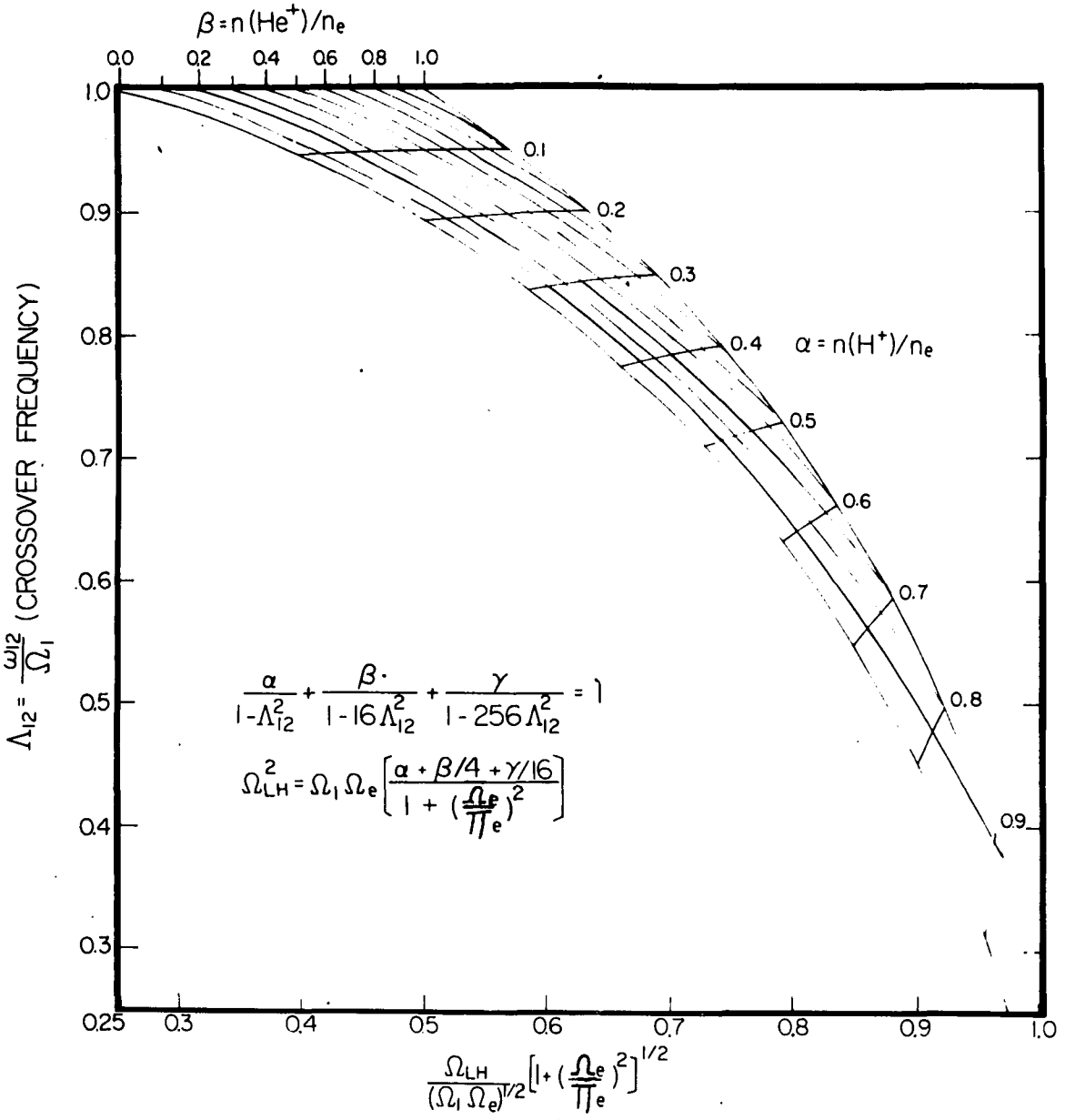

FIGURE 10

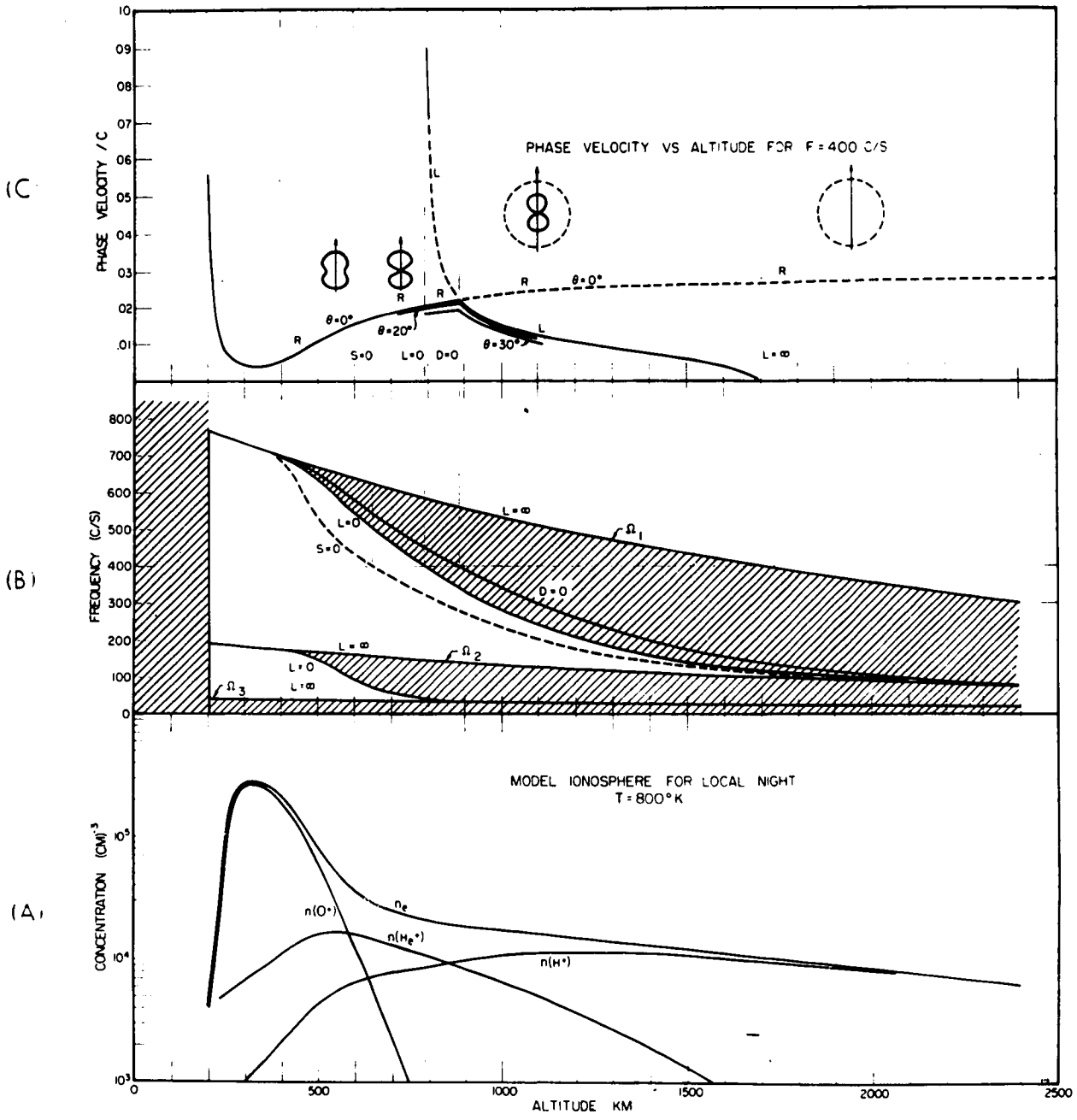
(C
PHASE VELOCITY VS ALTITUDE FOR F = 400 C/S
PHASE VELOCITY / C
θ=0°
θ=20°
θ=30°
S=0
L=0
D=0
L=∞
(B)
FREQUENCY (C/S)
Ω1
Ω2
Ω3
(A)
MODEL IONOSPHERE FOR LOCAL NIGHT
T = 800°K
CONCENTRATION (CM)⁻³
n(O⁺)
nₑ
n(Hₑ⁺)
n(H⁺)
ALTITUDE KM

FIGURE 11

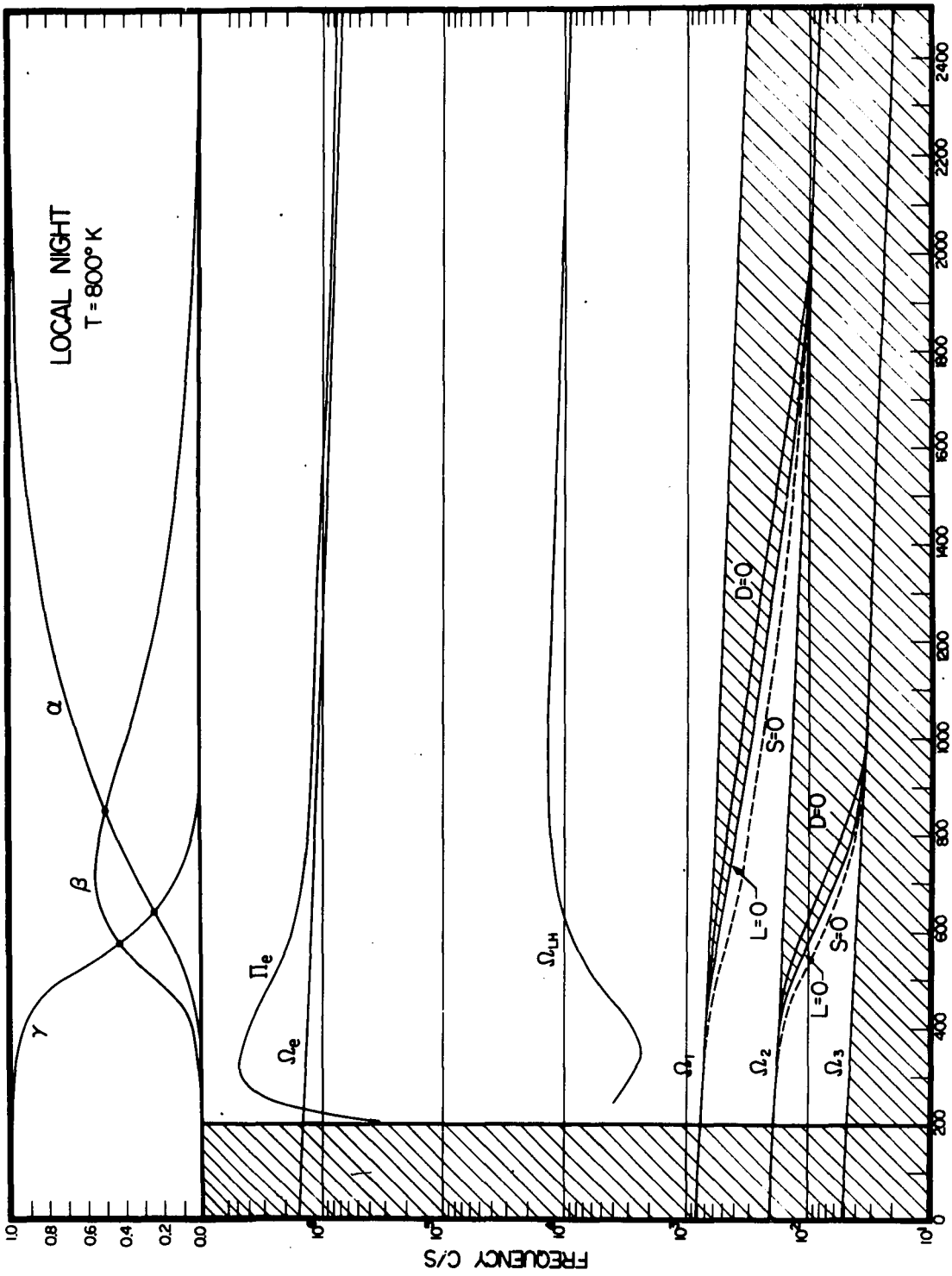
LOCAL NIGHT
T = 800° K
α
β
γ
Π_e
Ω_e
Ω_{LH}
Ω_1
Ω_2
Ω_3
L=0
S=0
D=0
L=0
S=0
D=0
1.0
0.8
0.6
0.4
0.2
0.0
10^2
10^1
10^0
10^{-1}
10^{-2}
FREQUENCY C/S
0
200
400
600
800
1000
1200
1400
1600
1800
2000
2200
2400
ALTITUDE KM

FIGURE 12

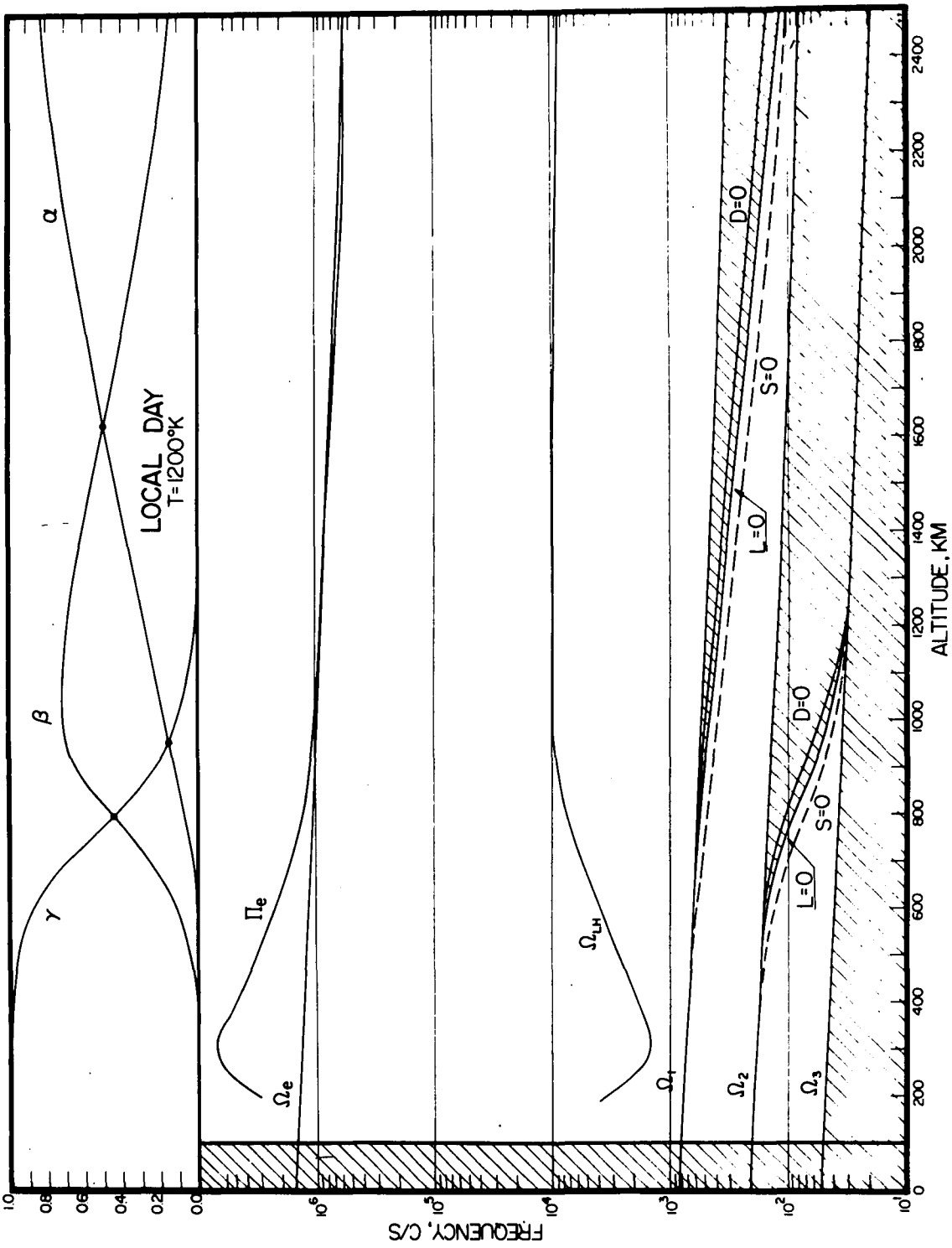
LOCAL DAY
T=1200°K
α
β
γ
Π_e
Ω_e
Ω_{LH}
Ω_1
Ω_2
Ω_3
L=0
D=0
S=0
FREQUENCY, C/S
ALTITUDE, KM

FIGURE 13

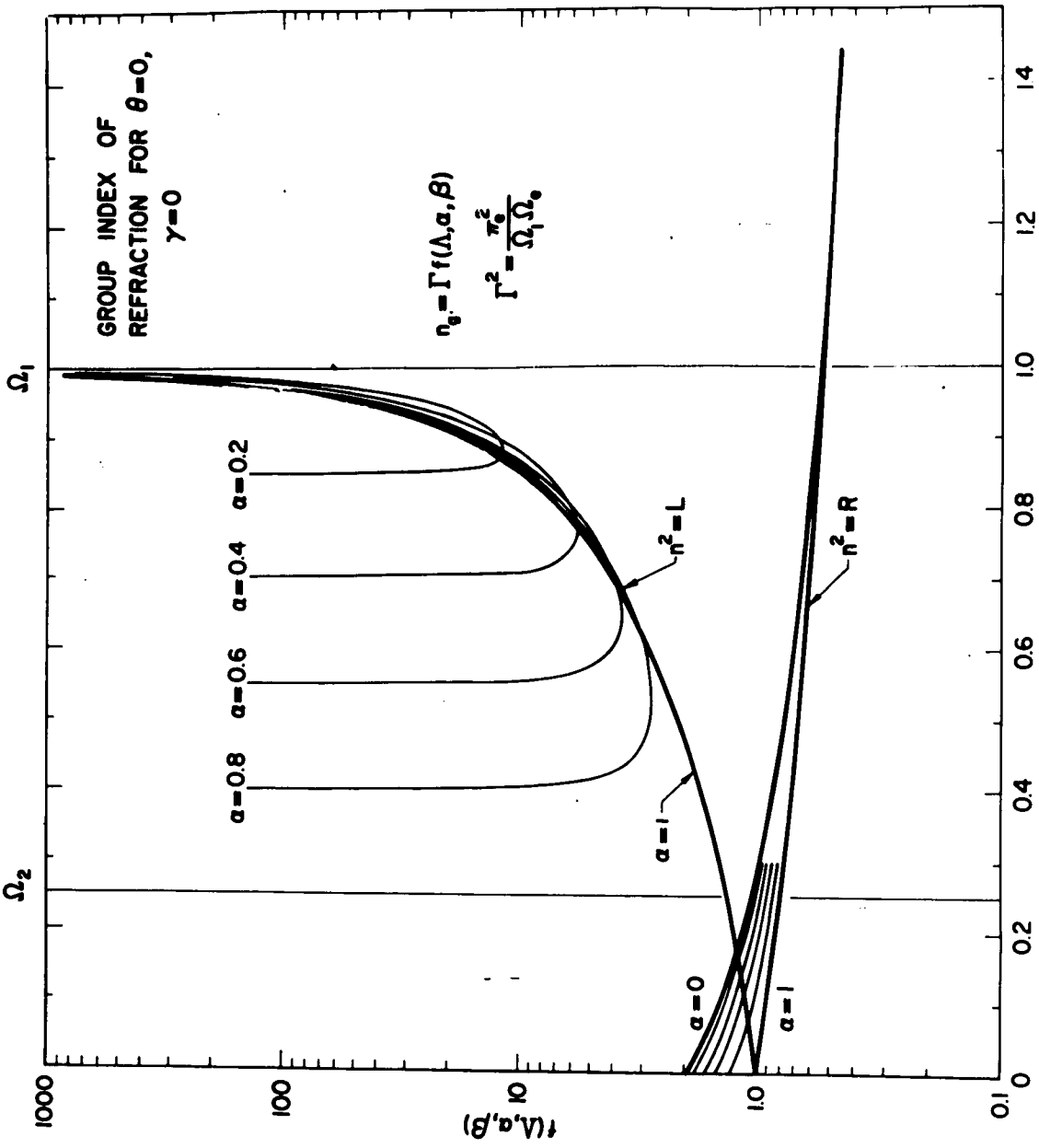
GROUP INDEX OF
REFRACTION FOR θ=0,
γ=0
$n_g = \Gamma f(\Lambda, a, \beta)$
$\Gamma^2 = \frac{\pi_e^2}{\Omega_1 \Omega_e}$
Ω_1
Ω_2
a=0.2
a=0.4
a=0.6
a=0.8
a=1
$n^2=L$
$n^2=R$
a=0
a=1
1000
100
10
1.0
0.1
f(Λ,a,β)
0
0.2
0.4
0.6
0.8
1.0
1.2
1.4
$\Lambda = \omega/\Omega_1$

FIGURE 14

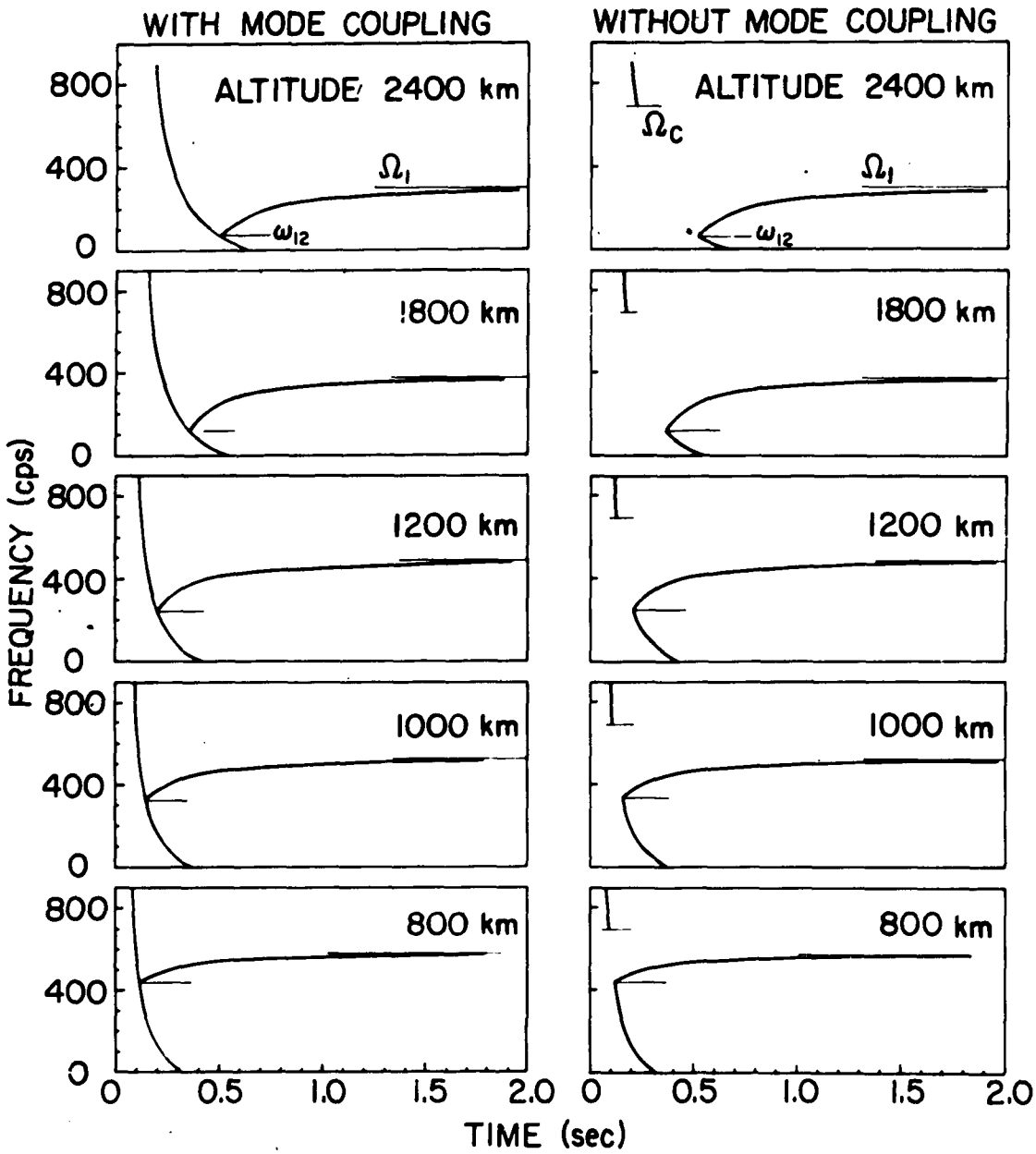
WITH MODE COUPLING
WITHOUT MODE COUPLING
ALTITUDE 2400 km
ALTITUDE 2400 km
Ω_1
ω_{12}
Ω_C
1800 km
1200 km
1000 km
800 km
FREQUENCY (cps)
800
400
0
0
0.5
1.0
1.5
2.0
TIME (sec)

FIGURE 15

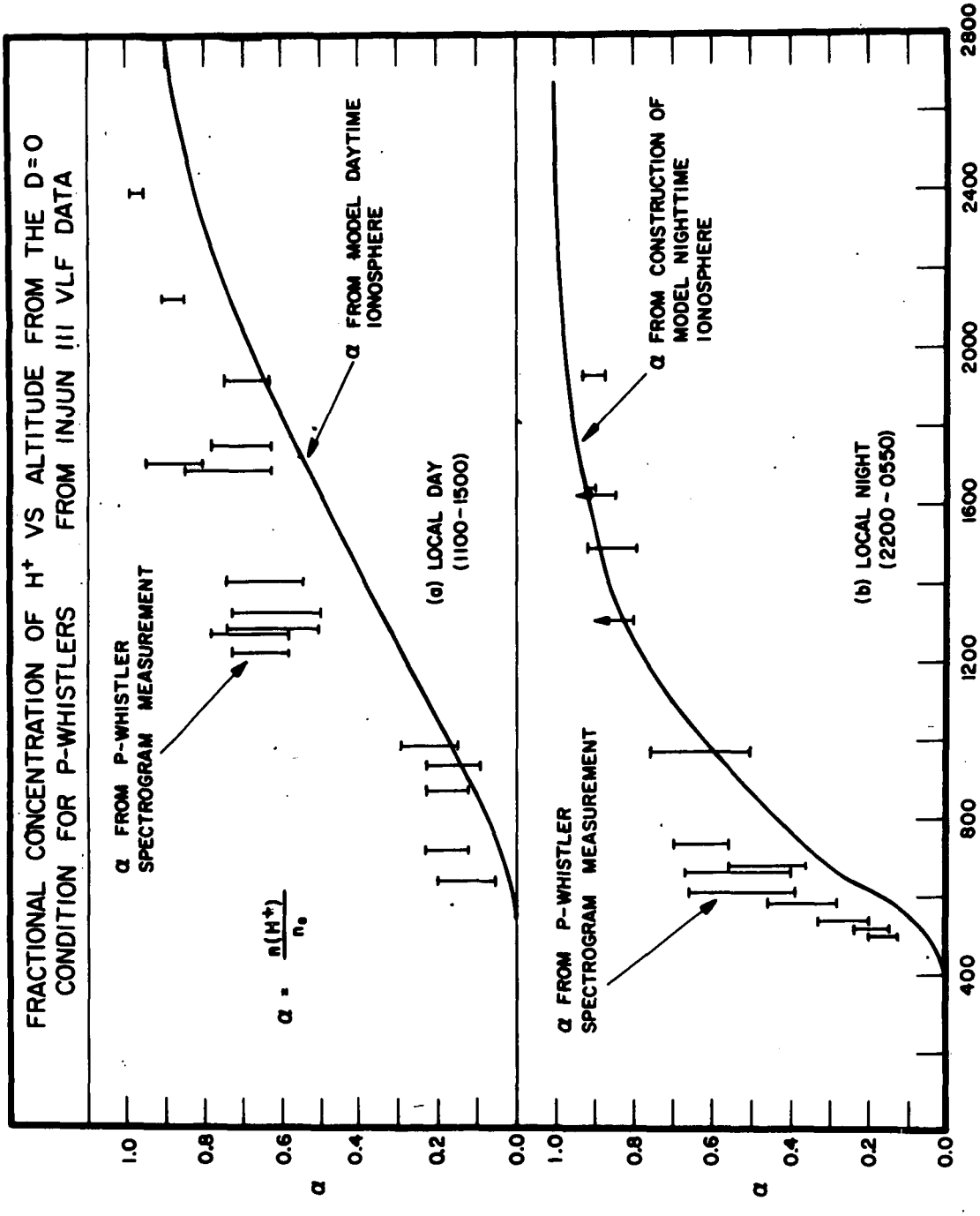
FRACTIONAL CONCENTRATION OF H+ VS ALTITUDE FROM THE D=0 CONDITION FOR P-WHISTLERS FROM INJUN III VLF DATA
α FROM P-WHISTLER SPECTROGRAM MEASUREMENT
α = n(H+)/ne
α FROM MODEL DAYTIME IONOSPHERE
(a) LOCAL DAY (1100-1500)
α FROM CONSTRUCTION OF MODEL NIGHTTIME IONOSPHERE
α FROM P-WHISTLER SPECTROGRAM MEASUREMENT
(b) LOCAL NIGHT (2200-0550)
α
ALTITUDE, KM
400
800
1200
1600
2000
2400
2800
0.0
0.2
0.4
0.6
0.8
1.0

FIGURE 16

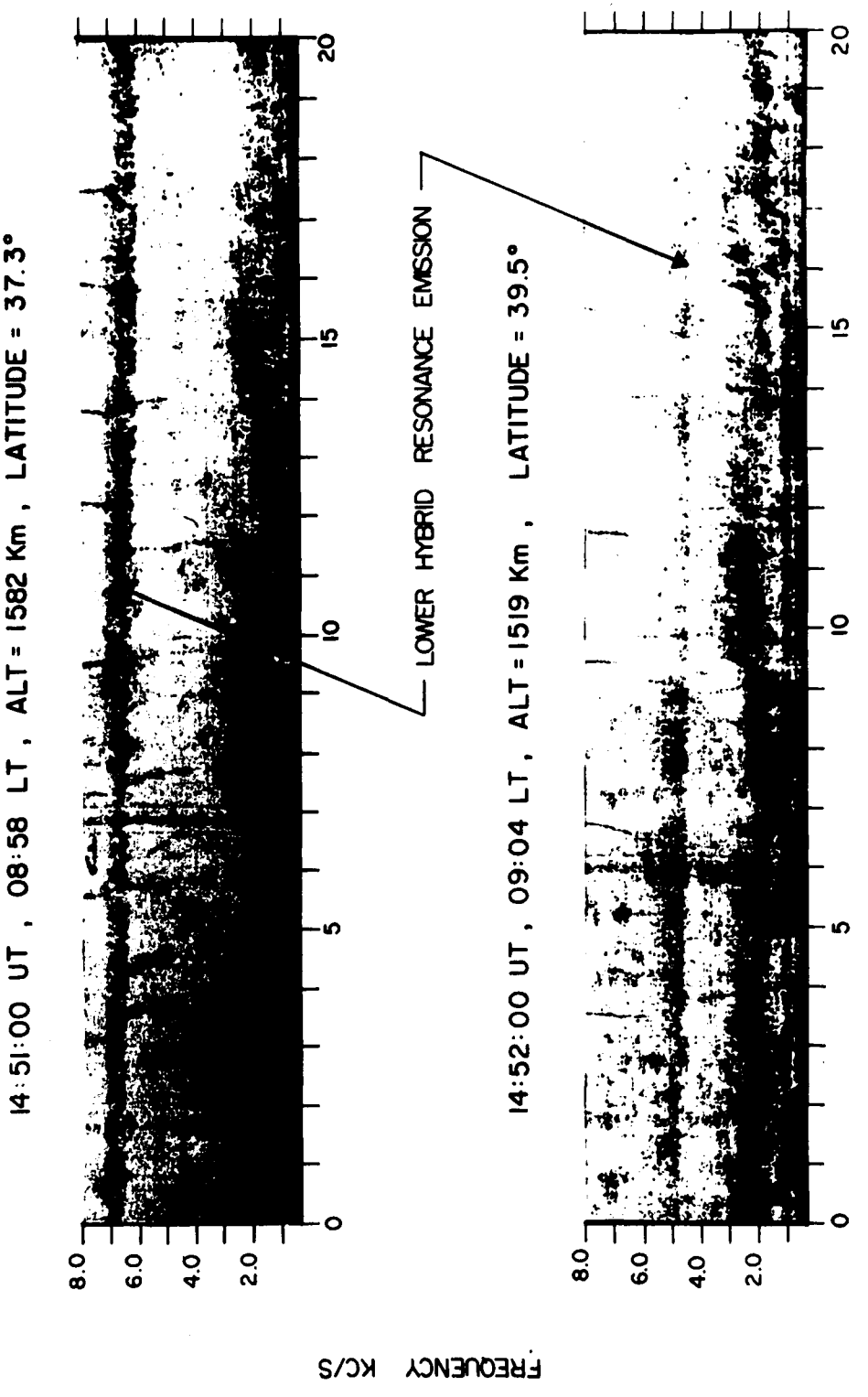
14:51:00 UT , 08:58 LT , ALT = 1582 Km , LATITUDE = 37.3°
14:52:00 UT , 09:04 LT , ALT = 1519 Km , LATITUDE = 39.5°
LOWER HYBRID RESONANCE EMISSION
FREQUENCY KC/S
8.0
6.0
4.0
2.0
0
5
10
15
20
TIME (SEC)

FIGURE 17

JAN. 14, 1963 10:46:10 UT, 05:20LT, ALTITUDE = 640 Km
L = 7.2 Ω_1 = 675 c/s.

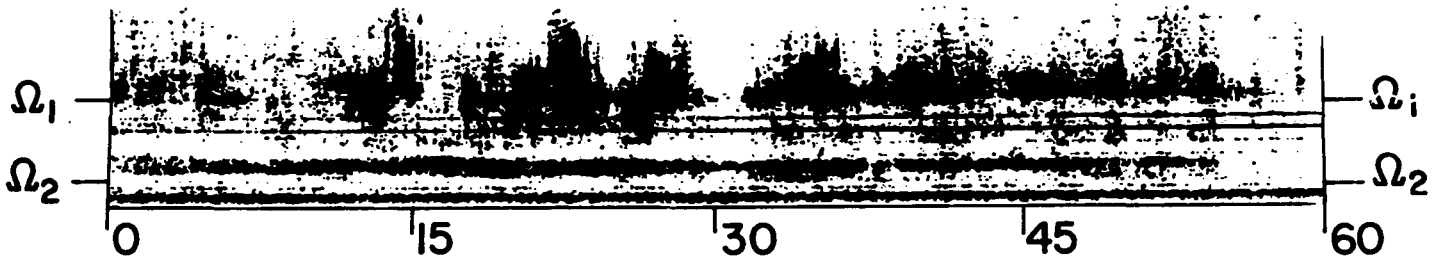

JAN. 17, 1963, 10:24:00 UT, 05:11LT ALTITUDE = 527 Km
L = 9.9 Ω_1 = 725 c/s.

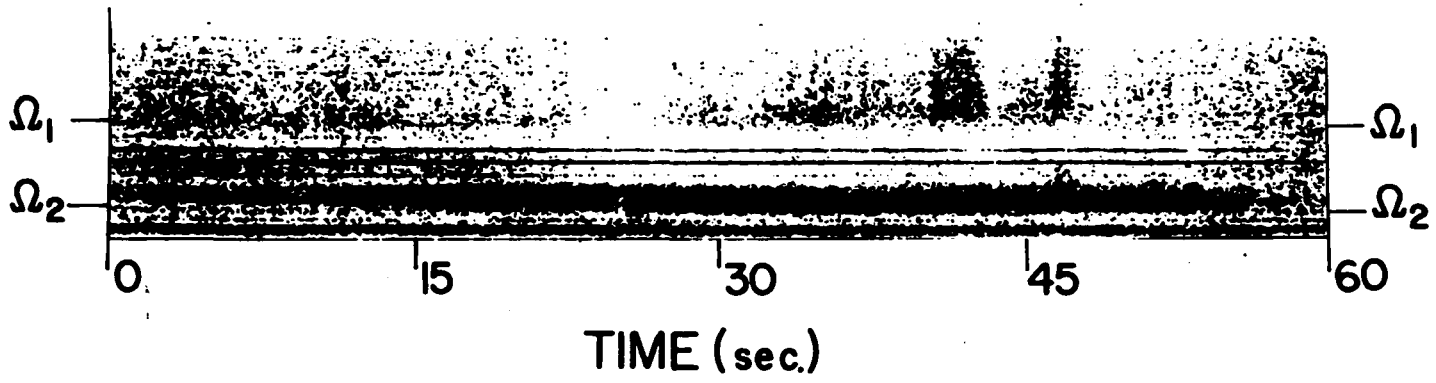

FIGURE 18